# Performance Analysis of Joint NOMA and JT-CoMP Based on Stienen Model

Yunpei Chen, Martin Haenggi, *Fellow, IEEE*, Qi Zhu, Caili Guo, *Senior Member, IEEE*, Yifei Yuan, *Fellow, IEEE*, Zhuhua Hu, *Senior Member, IEEE*, and Xiaohui Li, *Member, IEEE*

***Abstract*— For fifth-generation wireless networks to transition to sixth-generation wireless networks, the integration of coordinated multipoint (CoMP) and non-orthogonal multiple access (NOMA) techniques is expected to overcome new challenges and enhance performance compared to the CoMP or NOMA scheme. The joint-transmission CoMP (JT-CoMP) technique is a typical technical implementation of the CoMP scheme. In this study, we investigate a downlink network with a joint JT-CoMP-NOMA scheme. Based on the generalized Stienen model from stochastic geometry, we divide far and near NOMA user equipment (UE) and develop a theoretical framework to analyze the system performance. Expressions for the coverage probabilities and average achievable rates of two types of UEs (named CoMP and non-CoMP UEs) are derived. By comparing analytical results with Monte Carlo simulations, we show that the approximations in the analytical derivations are tight. The impact of certain network parameters, such as the power allocation coefficient, on the system performance is also studied. Notably, the developed transmission scheme is shown to outperform the NOMA-only and the JT-CoMP-only schemes.**

***Index Terms*— Non-orthogonal multiple access, joint-transmission coordinated multipoint, Stienen model, coverage probability, average achievable rate.**

Received 14 August 2024; revised 23 January 2025; accepted 21 February 2025. Date of publication 6 March 2025; date of current version 12 June 2025. This work was supported in part by Jiangsu Provincial Key Research and Development Program under Grant BE2022068-2, in part by the National Natural Science Foundation of China under Grant 62361024, in part by the Scientific Research Foundation of Hainan Tropical Ocean University under Grant RHDRCZK202537, in part by the Key Research and Development Project of Hainan Province under Grant ZDYF2024GXJS021, in part by the Fundamental Research Program of Shanxi Province under Grant 202203021212290, and in part by the Research Project Supported by Shanxi Scholarship Council of China under Grant 2023-053. The associate editor coordinating the review of this article and approving it for publication was L.-C. Wang. *(Corresponding author: Qi Zhu.)*

Yunpei Chen is with the School of Marine Information Engineering and the Yazhou Bay Innovation Institute, Hainan Tropical Ocean University, Sanya 572022, China, also with the School of Communication and Information Engineering, Nanjing University of Posts and Telecommunications, Nanjing 210003, China, and also with the Chief Engineer's Office, China Information Consulting and Designing Institute Company Ltd., Nanjing 210000, China (e-mail: 18913823955@189.cn).

Martin Haenggi is with the Department of Electrical Engineering, University of Notre Dame, Notre Dame, IN 46556 USA (e-mail: mhaenggi@nd.edu).

Qi Zhu and Xiaohui Li are with Jiangsu Key Laboratory of Wireless Communications, Nanjing University of Posts and Telecommunications, Nanjing 210003, China (e-mail: zhuqi@njupt.edu.cn; 20240035@njupt.edu.cn).

Caili Guo is with Beijing Key Laboratory of Network System Architecture and Convergence, School of Information and Communication Engineering, Beijing University of Posts and Telecommunications, Beijing 100876, China (e-mail: guocaili@bupt.edu.cn).

Yifei Yuan is with the Future Mobile Technology Laboratory, China Mobile Research Institute, Beijing 100053, China (e-mail: yuanyifei@chinamobile.com).

Zhuhua Hu is with the School of Information and Communication Engineering, Hainan University, Haikou 570228, China (e-mail: eagler_hu@hainanu.edu.cn).

Digital Object Identifier 10.1109/TWC.2025.3545922

## I. Introduction

### A. Motivation and Related Studies

With fifth-generation (5G) wireless networks being deployed worldwide, many studies have started to envision forms of sixth-generation (6G) wireless networks and to examine their corresponding application scenarios, demands, and key technologies. Although the research on 6G wireless networks is in the early stage, future wireless communication systems are expected to be smart, continuing the transformation of society from connected people and things to connected intelligence [1], [2], [3]. Due to its nondeterministic nature, interference, especially intercell interference (ICI), does serious harm to network performance. The standard solution of orthogonal multiple access limits the interference but comes at the cost of using increased spectral resources. Hence, to address the limitations of previous generation wireless networks, more advanced radio access technologies, such as coordinated multipoint (CoMP) and non-orthogonal multiple access (NOMA), have been widely investigated for 5G wireless networks. In the future, these technologies will be further developed and suitably adopted in 6G wireless networks. Integrating these technologies is expected to significantly enhance the performance.

CoMP techniques can reduce ICI and improve cell-edge coverage and throughput. Therefore, they were introduced by the Third-Generation Partnership Project (3GPP) in Release 11 of its technical specifications [4] to solve various issues of radio resource management in 5G wireless networks and beyond. The operation mode of CoMP comprises two categories: i) the fundamental interference avoidance mode (coordinated scheduling and beamforming) and ii) the more complex diversity gain mode [5]. As a typical mode, the joint-transmission CoMP (JT-CoMP) technique has attracted intense interest from both industry and academia. Generally, in the traditional JT-CoMP scheme, the same data are transmitted from multiple cell sites, which is more practical than other CoMP operation modes. In [6], the performance of the JT-CoMP technique in dense cellular networks was investigated based on stochastic geometry, and both outage probability and normalized goodput were derived. In [7], utilizing tools from stochastic geometry, an integral expression of coverage probability was derived for heterogeneous cellular networks employing the JT-CoMP scheme.

Considering its ability to improve spectral efficiency, enhance connectivity, and reduce transmission latency, the NOMA technique has been widely investigated for 5G wireless networks and beyond [8]. In contrast to conventional orthogonal multiple access (OMA) techniques, the NOMA

scheme lets some users share the same resource blocks. Although industry and academia have developed many specific technical implementations of the NOMA scheme [9], the power-domain NOMA technique, which was first proposed, is a promising candidate in the study of next-generation multiple access techniques for 6G wireless communication networks [10]. In the following sections of this paper, NOMA refers to power-domain NOMA, unless otherwise stated. In [11], using stochastic geometry, analytical results of the outage probability and ergodic data rate in a general multiuser single-cell NOMA scenario were obtained. In [12], for dense wireless networks, considering a two-user pairing NOMA scheme, the outage probability and average achievable rate in a multicell scenario were evaluated using stochastic geometry. In [13], considering the in-disk, which is the largest disk centered at a base station (BS) that fits inside its Voronoi cell, three models for user pairing in a NOMA scheme were proposed. The coverage of the typical user inside the in-disk was analyzed.

To further enhance user-access capability and improve the spectral efficiency performance, the integration of the JT-CoMP and NOMA techniques [14] has been studied recently as a promising paradigm for future wireless communication systems. In [15], the outage probability of a downlink JT-CoMP network was derived for an opportunistic NOMA technique. The network model includes some access points (APs) and many users, where all users comprise one NOMA group. The performance analysis was simple owing to the investigation of only one NOMA group. In [16], the outage probability and ergodic rate of a cell-edge user, called a CoMP user, were derived. The studied system model consists of two adjacent cells and three users, where each BS in the corresponding cell combines its near and common cell-edge users into a NOMA group. Specifically, two NOMA groups were considered in the study. In [17], the outage performances of near and cell-edge users were analyzed by combining the downlink JT-CoMP technique with a NOMA network. In this combined scheme, when two users are paired into a NOMA group, only three BSs are considered and support a cell-edge user cooperatively, with each BS individually communicating with a near user. Specifically, the BSs are assumed to form an equilateral triangle. In [18], the outage probabilities achieved by two types of users were obtained using a downlink JT-CoMP system equipped with a NOMA scheme. The BS locations are modeled using a homogeneous Poisson point process (PPP). Moreover, the PPP is the parent process of a Poisson cluster process (PCP), which is used to model near users. In one PCP cluster, a fixed number of near users are randomly and uniformly distributed in a disk centered at the corresponding BS. Cell-edge users, i.e., CoMP users, are defined as users whose distances from all BSs exceed a predefined value. Simultaneously, each CoMP user invites the BSs whose distances are shorter than another predefined value to serve it cooperatively. Single CoMP and near users in the cluster of the corresponding invited BS compose a NOMA group. Note that the system model is simple and quasi-stochastic, considering that the two predefined values are determinate and fixed and that CoMP users are unassociated with the PCP (all users are not generated by the same point process). In [19], based on a system model similar to that in [18] (having an identical network topology but opposite link directions), the outage probabilities and ergodic rates of two types of users were derived for an uplink JT-CoMP system equipped with a NOMA scheme. In addition to the aforementioned studies, research on integrating the NOMA and JT-CoMP techniques has expanded. In [20], the outage performance of a downlink JT-CoMP system combined with a multi-tier NOMA network was analyzed. This network model, which includes some APs and many users, implements a multi-tier NOMA strategy, wherein after a designed scheduling, each tier is regarded as an individual observation similar to that in [15]. In [21], the average ergodic rates of downlink heterogeneous cloud radio access networks were evaluated. These networks consist of two tiers of remote radio heads (RRHs) and integrate the JT-CoMP and NOMA techniques. Moreover, each tier of the developed model [21] considers a two-user NOMA group configuration, similar to that in [16]. Adopting the approach used in [16], the performances of four disjoint groups of users were analyzed. In addition, in [22] based on the integration of CoMP and NOMA, the joint user clustering and power allocation issue was investigated for the two-BS scenario. In [23], for the NOMA-enabled JT-CoMP, the optimal decoding order for the sum rate maximization problem was proved in the scenario where two BSs and two users were given. In [24], based on the application of network NOMA technique to CoMP systems, the precoding design for downlink scenarios with two BSs equipped with multiple antennas was studied considering quasi-degraded channels.

As mentioned above, many existing studies confirm the performance gain of a joint NOMA and JT-CoMP scheme. However, considering the realistic deployment of wireless networks and the feasibility of performance analysis based on stochastic geometry, some drawbacks of these studies should be addressed. The specific issues are as follows:

1) As elaborated in [6], [7], [11], [12], and [13], the performance analysis of the JT-CoMP or NOMA scheme is based on the user-centric and multicell characteristics of wireless networks. Therefore, the integrated JT-CoMP and NOMA scheme should be studied in multicell and multi-NOMA group scenarios. In general, when a one-tier wireless network is modeled in stochastic geometry, all user points must be generated by the same homogeneous random process. Note that in [15] and [20], only one NOMA group was considered. In [16], [17], and [21], only two or three cooperating BSs/RRHs were considered. Consequently, the results of these studies lack generalizability. Additionally, although the system models in [18] and [19] are multicell and multi-NOMA group models, user points are generated by two separate point processes: a PCP for near users and a PPP for cell-edge users. Therefore, the validity of the outcomes of [15], [16], [17], [18], [19], [20], and [21] should be carefully reviewed and reconsidered.
2) Note that in [15], [16], [17], [18], [19], [20], and [21], some detailed preconditions of the scheduling strategy were commonly assumed as part of the system model

before the formal performance analysis. For example, in [15] and [20], specific AP selection algorithms were applied to system models. Clearly, such artificial precondition affects the generality of the results of the performance analysis. In [17], [18], and [19], regardless of the area of a random cell, two determinate and fixed values were established to divide users into near and cell-edge users. However, only making this radius a function of the BS distances can ensure that the division reflects the fact that the cell edge is defined based on the shape and area of the cell.

3) A persistent belief is that coverage/outage performance and data rate are the two primary indicators that must be focused on when investigating the spectral efficiency of wireless networks. In [6], [7], [11], [12], and [13], in the performance analysis of either the JT-CoMP or the NOMA scheme, both coverage/outage probabilities and ergodic data rates of various types of users were derived. However, as discussed previously, few studies on the performance analysis of an integrated JT-CoMP and NOMA scheme have provided analytical results of these two indicators for both near and cell-edge users.
4) The JT-CoMP and NOMA techniques are the bases of this integration. In the existing literature, numerous numerical results have verified that the JT-CoMP or NOMA technique can outperform the conventional OMA scheme. Therefore, comparing the NOMA-only and the JT-CoMP-only technique with an integrated JT-CoMP and NOMA scheme is more relevant than comparing with the conventional OMA technique. However, the studies in [15], [16], [17], [18], [19], [20], and [21] mainly focused on the latter.

### B. Contributions

To further investigate and effectively utilize a joint NOMA and JT-CoMP scheme for 6G wireless networks, a sensible model is required for their representation. Moreover, based on a theoretical framework, the system performance should be analyzed thoroughly. An analytical solution of the performance is important. Along with an effective numerical comparison, it is beneficial for assisting system operations.

In this study, we aim to address the aforementioned issues and consider a downlink multicell network employing an integrated JT-CoMP and NOMA scheme. The main contributions of this study are as follows:

1) The BSs and user equipments (UEs) are modeled by two homogeneous PPPs. Subsequently, based on the generalized Stienen model from stochastic geometry [25], an elegant network model is established. In contrast to the UEs in [18] and [19], the distribution of UEs in the network model follows only one PPP. The model in [18] has two properties that make it less realistic: It rigidly assumes that users are pre-determined to be NOMA or CoMP users, and it allows for the possibility that NOMA users served by one BS may actually be lying in another BS's Voronoi cell–even though these users are declared "*near*" to the further BS. This similarly applies to [17] and [19]. In contrast, the generalized Stienen model is used to divide the far and near NOMA UEs simply and consistently.
2) Based on the integration of the JT-CoMP and NOMA features, the network model has two types of UEs: far NOMA UEs (as CoMP UEs), and near NOMA UEs (as non-CoMP UEs), respectively. The system performance for these two types of UEs are evaluated by deriving expressions of the coverage probability and average achievable rate. Considering the Laplace transform of the cumulative ICI, the approach for the typical user inside Stienen disk within the generalized Stienen model (i.e., the typical non-CoMP UE as conditioned version of the typical user in this study), is different from that for the typical user within the usual PPP model without Stienen disks. We provide a sound mathematical foundation for the detailed procedure of the former approach for the first time. Moreover, an improved approximation of one key variable in the procedure of the former approach is given in this study, compared to other studies [13], [26], [27].
3) In this study, numerous comparisons between analytical results and Monte Carlo simulations validate that the approximations in the derivations of expressions are tight. The impact of certain network parameters, such as the power allocation coefficient, on the system performance is numerically demonstrated. Significantly, we develop insights by comprehensively comparing the NOMA, JT-CoMP, and integrated JT-CoMP and NOMA schemes in terms of the performance gain of the overall system.

### C. Organization

The remainder of this paper is organized as follows: In Section II, we describe the system model and provide some necessary preliminaries for the evaluation. The derivation of the coverage probabilities for CoMP and non-CoMP UEs is presented in Section III. In Section IV, the average achievable rates of the two types of UEs are presented. The numerical and simulation results are discussed in Section V. Finally, Section VI concludes the paper.

## II. System Model and Preliminaries

Based on the categorization of UEs into CoMP and non-CoMP UEs, we introduce the joint NOMA and JT-CoMP scheme. To be specific, the non-coherent JT-CoMP[1] is considered in this work. Finally, some necessary preliminaries for evaluating the system performance are presented.

### A. Network Model

In this study, we consider a downlink network. The BS locations in the Euclidean plane are assumed to follow a PPP $\Phi = \{\chi_1, \chi_2, \ldots\}$ with intensity $\lambda$. The UEs form another PPP that is independent of $\Phi$. We assume that the intensity

[1]Note that there are two types of JT-CoMP, namely non-coherent JT-CoMP and coherent JT-CoMP. Neither tight synchronization nor prior phase mismatch correction is required in non-coherent JT-CoMP [28]. Because non-coherent JT-CoMP is more practical than coherent JT-CoMP, we utilize the non-coherent JT-CoMP in this work.

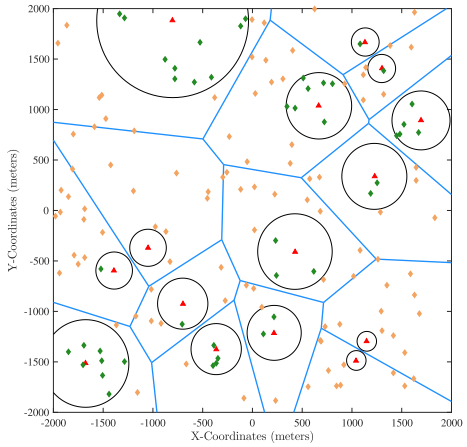


Fig. 1. Downlink network modeled by generalized Stienen model. Red triangles represent BSs. Blue lines represent boundaries of Voronoi cells. Black circles represent boundaries of Stienen disks. Green diamonds inside Stienen disks represent non-CoMP UEs. Orange diamonds outside Stienen disks represent CoMP UEs. All UEs are distributed according to a single PPP.

of the PPP of the UEs is much higher than $\lambda$ such that a sufficient number of UEs can always exist to form a NOMA group within each cell. A UE is associated with the nearest BS. Consequently, according to stochastic geometry, a Poisson-Voronoi tessellation [25] can be used to form the resulting association correspondence of this network model. As shown in Fig. 1, each Voronoi cell represents the region covered by its corresponding BS, where the associated UEs falls. Without loss of generality, we analyze the typical user in this study [25], [29], assumed at the origin $o$. If the typical user is served as a CoMP or non-CoMP UE, it is called the typical CoMP or non-CoMP UE, respectively. We order the BSs of $\Phi$ in increasing order of distance to the typical user.

In the network, all BSs and UEs are equipped with a single antenna [15], [16], [17], [18], [19], [20], [21]. All cells transmit data using the same frequency resources with frequency reuse factor 1. The channel power gain $h$ from a BS to the associated UE includes two factors: propagation path loss and independent random channel effects. To be specific, let $h = r^{-\alpha} g$ where $r$ is the distance between a BS and UE, $\alpha > 2$ is the path loss exponent, and $g$ represents the random channel effects, modeled as flat Rayleigh fading. Hence, the probability density function (PDF) of $g$ is $f_g(x) = \beta e^{-\beta x}$ for $x > 0$, where the mean of $g$ is $\frac{1}{\beta}$. Additive white Gaussian noise (AWGN) with zero mean and constant variance $\sigma^2$ is considered at the UEs.

### B. Transmission Scheme

The NOMA scheme is adopted as the multiple access technique in the network. Considering the processing complexity and latency of successive interference cancellation (SIC) at receivers in realistic scenarios, a two-UE NOMA group configuration is assumed. This configuration has been standardized in the 3GPP long-term evolution advanced [30]. Let $P_t$ denote the total transmission power of a BS in the system bandwidth. While a dynamic power allocation has been shown to improve system performance such as weighted-sum-rate and sum-rate utilities [31], and energy efficiency [32], it requires a high signaling overhead. However, a fixed-power allocation strategy is still of practical interest, notably because of its capability to achieve near-optimal performance with a lower signaling overhead. Fixed power allocation is utilized in the network. Generally, UEs with different channel conditions are recommended to form a NOMA group for user pairing. In terms of average channel conditions, UEs with poor channel conditions are referred to as far NOMA or cell-edge UEs. UEs with good channel conditions are referred to as near NOMA or cell-center UEs. Herein, the power allocated to a near-NOMA UE in a two-UE NOMA group is denoted by $\epsilon P_t$. The power allocated to a far-NOMA UE is $(1-\epsilon) P_t$, where $\epsilon \in (0, 0.5)$ is the power allocation coefficient.[2] And it is assumed that the proceeding of SIC would be implemented successfully in the network.[3]

In terms of system performance (e.g., sum data rate [11], total backlog, and delay [33]), the necessary disparity in the channel conditions between the UEs in one group is an aspect to be focused on in NOMA networks. Determining suitable criteria for clearly dividing far and near NOMA UEs would be important for evaluating the system performance of the NOMA scheme based on stochastic geometry. In this study, based on the constructed Poisson-Voronoi tessellation, we employ Stienen disks to implement such division. As shown in Fig. 1, the BS points generated by $\Phi$ are used as seeds to construct a Voronoi tessellation. Subsequently, around each point, a disk of radius equal to the product of the distance to the closest neighbor of the BS and a scalar factor $\Delta$ is placed. Such a disk is called Stienen disk.[4] Here, we utilize the generalized Stienen model with $\Delta \in (0, 0.5]$. For $\Delta = 0.5$, the disk becomes the classical Stienen disk [25]. Based on the PPP of the BSs, two mutual closest BSs have the same radii of their Stienen disks, i.e., the radii of the Stienen disks are not independent. UEs who lie inside a disk will be served as near-NOMA UEs, while those outside all disks are far-NOMA UEs. The radius of the Stienen disk around the closest BS to the origin (i.e., the typical user) is denoted as $R_{\mathrm{S}}$.

To mitigate the detrimental ICI, the CoMP scheme was adopted by the 3GPP in Release 11. Among the various technical implementations of the CoMP technique, the JT-CoMP scheme is the most practical. In this study, we focus on the integration of the JT-CoMP and NOMA (JT-CoMP-NOMA) features in a downlink network. In Fig. 2, the joint JT-CoMP-NOMA scheme is illustrated. A far NOMA UE is included in two different NOMA groups (NOMA Group 1 and NOMA Group 2, belonging to BS1 and BS2, respectively). In the network for the far NOMA UE, BS1 is the nearest BS,

[2]In practice, the dynamic resource allocation is often implemented. Obviously, $\epsilon$ is one of the key parameters for the joint NOMA and JT-CoMP scheme. There is an optimal value of $\epsilon$ that maximizes the system performance. Thus our work engenders the formulation of concrete optimization problems whose solution will benefit the dynamic deployment of joint NOMA and JT-CoMP systems.

[3]It is a common assumption to the pair near and far NOMA users on the distances. Moreover, by virtue of the fixed power allocation and the Stienen model-based user pairing in this work, only binary knowledge whether the distance is above or below some threshold is required, rather than full knowledge of the average link attenuation. Specifically, channel state information (CSI) is not needed.

[4]The performance analysis should guide the decision which users should be paired in practice. Deciding on the optimum $\Delta$ could be viewed as an instance of this.

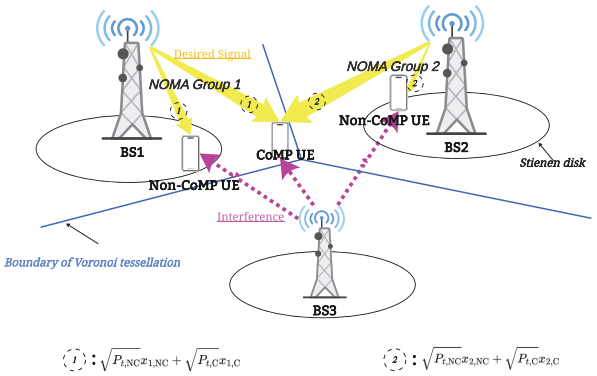


Fig. 2. JT-CoMP-NOMA scheme. One CoMP UE as far-NOMA UE and one non-CoMP UE as near-NOMA UE form a two-UE NOMA group.

whereas BS2 is the second-nearest BS. The far NOMA UE simultaneously receives the same message only from BS1 and BS2 over the same frequency resource. Hence, far-NOMA UEs are CoMP UEs, while near-NOMA UEs are non-CoMP UEs. Accordingly, there are only two types of UEs in the network, which we term Type-1 and Type-2 users. Type-1 users are far-NOMA users; they lie outside the Stienen disks and are served using CoMP. Type-2 users are near-NOMA non-CoMP users. Type-1 and Type-2 users are paired to form NOMA groups.[5]

The developed framework, as shown in Fig. 1 and 2, has two noteworthy features. Specifically, the first technical point is that the number of cooperative BSs that simultaneously transmit data to a CoMP UE is set to two. The larger the cluster size of the cooperative BSs being considered, the more overhead is required because of the cost of additional signal processing and increased feedback and signaling. A two-BS cluster size is practical due to its low complexity. Second, the number of UEs in the NOMA group is limited to two. In addition to the related interpretations provided at the beginning of this subsection, another important factor, namely the SIC decoding order must be considered for such a configuration. As highlighted in [14], the SIC decoding order for a CoMP UE should be the same for all NOMA groups formed in a particular CoMP set. In this study, the two-UE NOMA group configuration based on the Stienen model satisfies this criterion.

### C. Necessary Preliminaries

To avoid making the subsequent discussions difficult, some necessary mathematical preliminaries are recalled or provided below.

*Lemma 1 [34]:*

$$\int_x^\infty \frac{1}{1+u^a}du = \frac{x^{1-a}}{a-1}\cdot {}_2F_1\left(1, 1-a^{-1}; 2-a^{-1}; -x^{-a}\right)$$

*for $x > 0$ and $a > 1$. Here, ${}_2F_1(\alpha, \beta; \gamma; z)$ denotes the Gauss hypergeometric function.*

*Lemma 2: Let $X$ and $Y$ be independent exponential random variables with means $1/\alpha$ and $1/\beta$, respectively. For $a > 0$, $b > 0$ and $a\beta \neq b\alpha$, the PDF of $Z = aX + bY$ is $f_Z(z) = \frac{\alpha\beta}{a\beta - b\alpha}(e^{-\frac{\alpha z}{a}} - e^{-\frac{\beta z}{b}})$, $z \geq 0$.*

*Proof:* Follows from elementary probability. ■

Let $R_n$ denote the distance from the typical user to the $n$th nearest neighbor BS in the PPP $\Phi$. According to [25], [29], and [35], in the Euclidean plane, the PDFs of these distances are given as follows:

- $f_{R_1}(r) = 2\pi\lambda r e^{-\pi\lambda r^2}$
- $f_{R_n}(r) = \frac{2(\pi\lambda)^n}{(n-1)!} r^{2n-1} e^{-\pi\lambda r^2}$
- $f_{(R_1, R_2, \ldots, R_n)}(r_1, r_2, \ldots, r_n) = e^{-\pi\lambda r_n^2} 2(\pi\lambda)^n r_1 r_2 \cdots r_n$

Let $R_{\text{typ}}$ be the radius of the typical Stienen disk, which is the disk at an arbitrary location $u$ given that $u \in \Phi$. Then considering that the distance to the nearest neighbor can be denoted by $R_{\text{typ}}\Delta^{-1}$, the PDF of $R_{\text{typ}}$ can be derived as $f_{R_{\text{typ}}}(r) = 2\pi\lambda r\Delta^{-2} e^{-\pi\lambda\left(\frac{r}{\Delta}\right)^2}$ [26], [27]. Obviously, $R_{\text{S}}$ focused on in this study is different from $R_{\text{typ}}$. With a small loss in accuracy (as can be observed from simulations), $f_{R_{\text{typ}}}(r)$ is used as an approximation of the PDF of $R_{\text{S}}$, i.e., $f_{R_{\text{S}}}(r) \approx 2\pi\lambda r\Delta^{-2} e^{-\pi\lambda\left(\frac{r}{\Delta}\right)^2}$. Furthermore, the following lemma reveals the probability of the typical user lying in a Stienen disk.

*Lemma 3 [36]: Under the generalized Stienen model constructed using a Poisson-Voronoi tessellation, the probability of the typical user inside Stienen disk is $\Delta^2$ with a scalar factor $\Delta \in (0, 0.5]$.*

The probability in Lemma 3 can be interpreted as the covered area fraction of all Stienen disks. Since the Stienen disks do not overlap, it is straightforward to calculate the fraction of the area they cover [36].

## III. Coverage Probabilities

In this section, first, the transmitted signals at the cooperative BSs and received signals at the UEs are briefly presented. Subsequently, based on the expressions of the signal-to-interference-plus-noise ratio (SINR), the derivation of the coverage probabilities for the typical CoMP and non-CoMP UEs is provided.

### A. Transmitted and Received Signals

As shown in Fig. 2, we assume that the signals from BS1 and BS2 for the same CoMP UE are expressed as $x_{1,\text{C}}$ and $x_{2,\text{C}}$ respectively, with $\mathbb{E}\left[|x_{1,\text{C}}|^2\right] = \mathbb{E}\left[|x_{2,\text{C}}|^2\right] = 1$. The signals from BS1 and BS2 for the associated non-CoMP UEs are denoted as $x_{1,\text{NC}}$ with $\mathbb{E}\left[|x_{1,\text{NC}}|^2\right] = 1$ and $x_{2,\text{NC}}$ with $\mathbb{E}\left[|x_{2,\text{NC}}|^2\right] = 1$, respectively. Here, subscript "1" or "2" indicates the BS that the variable is related to. Subscripts "C" and "NC" indicate that the variable is intended for a CoMP UE outside Stienen disk and non-CoMP UE inside Stienen disk, respectively. The definitions of these subscripts are consistent and maintained throughout the paper. According to the joint JT-CoMP-NOMA scheme presented in Section II, $x_{1,\text{C}}$ and $x_{1,\text{NC}}$ are encoded at BS1 as the composite signal, $\sqrt{P_{t,\text{NC}}}x_{1,\text{NC}} + \sqrt{P_{t,\text{C}}}x_{1,\text{C}}$, where $P_{t,\text{NC}} = \epsilon P_t$ and $P_{t,\text{C}} = (1-\epsilon)P_t$ denote the powers allocated to the non-CoMP and

[5]In this work, a Type-1 user and a Type-2 user are picked uniformly at random to form a NOMA group. Since the area fraction of the Stienen disks is $\Delta^2$, which is at most 1/4, there are users outside the disks who cannot be paired. They are assumed to be served using conventional OMA using separate frequency resources.

CoMP UEs, respectively. At BS2, $x_{2,\mathrm{C}}$ and $x_{2,\mathrm{NC}}$ are encoded as the composite signal, $\sqrt{P_{t,\mathrm{NC}}}x_{2,\mathrm{NC}}+\sqrt{P_{t,\mathrm{C}}}x_{2,\mathrm{C}}$. Hence, the received signal at the CoMP UE can be expressed as

$$\begin{aligned}&(\sqrt{P_{t,\mathrm{NC}}}x_{1,\mathrm{NC}}+\sqrt{P_{t,\mathrm{C}}}x_{1,\mathrm{C}})\sqrt{h_{1,\mathrm{C}}}\\&+(\sqrt{P_{t,\mathrm{NC}}}x_{2,\mathrm{NC}}+\sqrt{P_{t,\mathrm{C}}}x_{2,\mathrm{C}})\sqrt{h_{2,\mathrm{C}}}\\&+\sum_{i>2}(\sqrt{P_{t,\mathrm{NC}}}x_{i,\mathrm{NC}}^{(i)}+\sqrt{P_{t,\mathrm{C}}}x_{i,\mathrm{C}}^{(i)})\sqrt{h_{i,\mathrm{C}}}+n_{\mathrm{C}}\\=&\underbrace{\sqrt{P_{t,\mathrm{C}}}(x_{1,\mathrm{C}}\sqrt{h_{1,\mathrm{C}}}+x_{2,\mathrm{C}}\sqrt{h_{2,\mathrm{C}}})}_{\text{desired signal}}\\&+\underbrace{\sqrt{P_{t,\mathrm{NC}}}(x_{1,\mathrm{NC}}\sqrt{h_{1,\mathrm{C}}}+x_{2,\mathrm{NC}}\sqrt{h_{2,\mathrm{C}}})}_{\text{interference from near NOMA UEs}}\\&+\underbrace{\sum_{i>2}(\sqrt{P_{t,\mathrm{NC}}}x_{i,\mathrm{NC}}^{(i)}+\sqrt{P_{t,\mathrm{C}}}x_{i,\mathrm{C}}^{(i)})\sqrt{h_{i,\mathrm{C}}}}_{\text{interference from other BSs}}+n_{\mathrm{C}}\,,\end{aligned}\tag{1}$$

where $n_{\mathrm{C}}$ denotes the AWGN and, $x_{i,\mathrm{NC}}^{(i)}$ and $x_{i,\mathrm{C}}^{(i)}$ are the transmitted signals from BS-$i$ to its associated non-CoMP and CoMP UEs (both not as the typical user), respectively. Considering the non-CoMP UE associated with BS1, the received signal at this UE can be represented as

$$\begin{aligned}&(\sqrt{P_{t,\mathrm{NC}}}x_{1,\mathrm{NC}}+\sqrt{P_{t,\mathrm{C}}}x_{1,\mathrm{C}})\sqrt{h_{1,\mathrm{NC}}}\\&+\sum_{i>1}(\sqrt{P_{t,\mathrm{NC}}}x_{i,\mathrm{NC}}^{(i)}+\sqrt{P_{t,\mathrm{C}}}x_{i,\mathrm{C}}^{(i)})\sqrt{h_{i,\mathrm{NC}}}+n_{\mathrm{NC}}\\=&\underbrace{\sqrt{P_{t,\mathrm{NC}}}x_{1,\mathrm{NC}}\sqrt{h_{1,\mathrm{NC}}}}_{\text{desired signal}}+\underbrace{\sqrt{P_{t,\mathrm{C}}}x_{1,\mathrm{C}}\sqrt{h_{1,\mathrm{NC}}}}_{\text{interference from far NOMA UE}}\\&+\underbrace{\sum_{i>1}(\sqrt{P_{t,\mathrm{NC}}}x_{i,\mathrm{NC}}^{(i)}+\sqrt{P_{t,\mathrm{C}}}x_{i,\mathrm{C}}^{(i)})\sqrt{h_{i,\mathrm{NC}}}}_{\text{interference from other BSs}}+n_{\mathrm{NC}}\,,\end{aligned}\tag{2}$$

where $n_{\mathrm{NC}}$ denotes the AWGN.

### B. Coverage for the Typical CoMP UE

In the system model of this study, when the typical user is served as a CoMP UE, it is called the typical CoMP UE. Based on the joint JT-CoMP-NOMA scheme, the received signal at the typical CoMP UE can be directly represented as that at the CoMP UE in Fig. 2. Then, the typical CoMP UE decodes $x_{1,\mathrm{C}}$ and $x_{2,\mathrm{C}}$ by treating $x_{1,\mathrm{NC}}$ and $x_{2,\mathrm{NC}}$ as interference. Based on (1), the SINR for the typical CoMP UE can be expressed as

$$\mathrm{SINR}_{\mathrm{C}}=\frac{P_{t,\mathrm{C}}h_{1,\mathrm{C}}+P_{t,\mathrm{C}}h_{2,\mathrm{C}}}{P_{t,\mathrm{NC}}h_{1,\mathrm{C}}+P_{t,\mathrm{NC}}h_{2,\mathrm{C}}+\sum_{i>2}P_th_{i,\mathrm{C}}+\sigma^2}\,,\tag{3}$$

where $I_{\mathrm{C}}=\sum_{i>2}P_th_{i,\mathrm{C}}=\sum_{i>2}P_tr_{i,\mathrm{C}}^{-\alpha}g_{i,\mathrm{C}}$ is the cumulative ICI from all other BSs (i.e., $\Phi$ excluding BS1 and BS2) to the typical CoMP UE. If $T_{\mathrm{C}}$ is defined as the SINR threshold for applying SIC successfully at a CoMP UE, the coverage probability for the typical CoMP UE can be expressed as

$$\begin{aligned}&\mathbb{P}\left[\mathrm{SINR}_{\mathrm{C}}>T_{\mathrm{C}}\right]\\&=\mathbb{P}\left[\left(\frac{P_{t,\mathrm{C}}-T_{\mathrm{C}}P_{t,\mathrm{NC}}}{r_{1,\mathrm{C}}^{\alpha}}g_{1,\mathrm{C}}\right.\right.\\&\left.\left.+\frac{P_{t,\mathrm{C}}-T_{\mathrm{C}}P_{t,\mathrm{NC}}}{r_{2,\mathrm{C}}^{\alpha}}g_{2,\mathrm{C}}\right)>\left(I_{\mathrm{C}}+\sigma^2\right)T_{\mathrm{C}}\right].\end{aligned}\tag{4}$$

For simplicity, we use $A=\frac{P_{t,\mathrm{C}}-T_{\mathrm{C}}P_{t,\mathrm{NC}}}{r_{1,\mathrm{C}}^{\alpha}}$, $B=\frac{P_{t,\mathrm{C}}-T_{\mathrm{C}}P_{t,\mathrm{NC}}}{r_{2,\mathrm{C}}^{\alpha}}$, and $C=\left(I_{\mathrm{C}}+\sigma^2\right)T_{\mathrm{C}}$. The coverage probability, $\mathbb{P}\left[\mathrm{SINR}_{\mathrm{C}}>T_{\mathrm{C}}\right]$, can be rewritten as $\mathbb{P}\left[\mathrm{SINR}_{\mathrm{C}}>T_{\mathrm{C}}\right]=\mathbb{P}\left[(Ag_{1,\mathrm{C}}+Bg_{2,\mathrm{C}})>C\right]$. $g_{1,\mathrm{C}}$ and $g_{2,\mathrm{C}}$ are independent and identically distributed (i.i.d.). According to Lemma 2, $\mathbb{P}\left[\mathrm{SINR}_{\mathrm{C}}>T_{\mathrm{C}}\right]$ is evaluated as

$$\begin{aligned}&\mathbb{P}\left[\mathrm{SINR}_{\mathrm{C}}>T_{\mathrm{C}}\right]\\&=\mathbb{P}\left[(Ag_{1,\mathrm{C}}+Bg_{2,\mathrm{C}})>C\right]\\&=1-\mathbb{P}\left[(Ag_{1,\mathrm{C}}+Bg_{2,\mathrm{C}})\le C\right]\\&=1-\int_0^C\frac{\beta}{A-B}\left(e^{-\frac{\beta z}{A}}-e^{-\frac{\beta z}{B}}\right)dz\\&=\frac{1}{A-B}\left(A\exp\left(-\frac{\beta}{A}C\right)-B\exp\left(-\frac{\beta}{B}C\right)\right).\end{aligned}\tag{5}$$

Note the random variables $r_{1,\mathrm{C}}$, $r_{2,\mathrm{C}}$, and $I_{\mathrm{C}}$ in the last step of (5). Additionally, random variable $R_{\mathrm{S}}$ is implicitly contained in (5), because the CoMP UE is outside Stienen disk according to the system model. Recalling the PDFs of $R_{\mathrm{S}}$ and joint distribution of $R_n$ presented in Section II, $\mathbb{P}\left[\mathrm{SINR}_{\mathrm{C}}>T_{\mathrm{C}}\right]$ can be expressed as (6), shown at the bottom of the next page, where $I'_{\mathrm{C}}=\sum_{i>2}r_{i,\mathrm{C}}^{-\alpha}g_{i,\mathrm{C}}$ is the normalized value of $I_{\mathrm{C}}$ in step (a). In stochastic geometry, the probability generating functional (PGFL) of a PPP is, for a function $\psi(x)$, $\mathbb{E}\left[\prod_{x\in\Phi}\psi(x)\right]=\exp\left(-\lambda\int_{\mathbb{R}^2}\left(1-\psi(x)\right)dx\right)$. Although $I'_{\mathrm{C}}$ is obtained on set $\Phi\backslash\{\mathrm{BS1},\mathrm{BS2}\}$ instead of $\Phi$, step (b) can follow from the PGFL approximately with the Laplace transform, $\mathcal{L}\left(\bullet\right)$, which is widely adopted in the literature [6], [12], [13], and [37]. In step (c),[6] the expectation is expressed as a triple integral over the region $V_{\mathrm{C}}$.

Accordingly, in the remainder of this subsection, $\mathcal{L}_{I'_{\mathrm{C}}}\left(\frac{\beta P_tT_{\mathrm{C}}}{P_{t,\mathrm{C}}-T_{\mathrm{C}}P_{t,\mathrm{NC}}}r_{1,\mathrm{C}}^{\alpha}\right)$ and $\mathcal{L}_{I'_{\mathrm{C}}}\left(\frac{\beta P_tT_{\mathrm{C}}}{P_{t,\mathrm{C}}-T_{\mathrm{C}}P_{t,\mathrm{NC}}}r_{2,\mathrm{C}}^{\alpha}\right)$ are explored. The former can be obtained by

$$\begin{aligned}&\mathcal{L}_{I'_{\mathrm{C}}}\left(\frac{\beta P_tT_{\mathrm{C}}}{P_{t,\mathrm{C}}-T_{\mathrm{C}}P_{t,\mathrm{NC}}}r_{1,\mathrm{C}}^{\alpha}\right)\\&=\mathbb{E}\left[\exp\left(-sI'_{\mathrm{C}}\right)\right]\Big|_{s=\frac{\beta P_tT_{\mathrm{C}}}{P_{t,\mathrm{C}}-T_{\mathrm{C}}P_{t,\mathrm{NC}}}r_{1,\mathrm{C}}^{\alpha}}\\&=\mathbb{E}\left[\exp\left(-s\sum_{i>2}r_{i,\mathrm{C}}^{-\alpha}g_{i,\mathrm{C}}\right)\right]\\&=\mathbb{E}\left[\prod_{i>2}\exp\left(-sr_{i,\mathrm{C}}^{-\alpha}g_{i,\mathrm{C}}\right)\right]\\&\overset{(a)}{=}\mathbb{E}\left[\prod_{i>2}\mathbb{E}\left[\exp\left(-sr_{i,\mathrm{C}}^{-\alpha}g\right)\right]\right]\\&\overset{(b)}{=}\exp\left(-2\pi\lambda\int_{r_{2,\mathrm{C}}}^{\infty}\left(1-\mathbb{E}\left[\exp\left(-sv^{-\alpha}g\right)\right]\right)vdv\right)\end{aligned}$$

[6]Note that $R_1$ and $R_2$ are dependent with the explicit joint PDF $f_{(R_1,R_2)}(r_1,r_2)$ presented in Section II. Also, $R_1$ and $R_{\mathrm{S}}$ are dependent. However, to simplify the analysis, we assume $R_{\mathrm{S}}$ to be independent of $R_1$ and $R_2$. The resulting error is minimal, as shown in the numerical results.

$$= \exp\left(-2\pi\lambda \int_{r_{2,\mathrm{C}}}^{\infty} \frac{\Gamma_{\mathrm{C}}}{\Gamma_{\mathrm{C}} + (v/r_{1,\mathrm{C}})^{\alpha}} v dv\right)\Bigg|_{\Gamma_{\mathrm{C}}=\frac{P_t T_{\mathrm{C}}}{P_{t,\mathrm{C}} - T_{\mathrm{C}} P_{t,\mathrm{NC}}}}$$

$$\overset{(c)}{=} \exp\left(-\pi\lambda r_{1,\mathrm{C}}^2 \Gamma_{\mathrm{C}}^{\frac{2}{\alpha}} \int_{\left(\frac{r_{2,\mathrm{C}}}{r_{1,\mathrm{C}}}\right)^2 \Gamma_{\mathrm{C}}^{-\frac{2}{\alpha}}}^{\infty} \frac{1}{1+u^{\frac{\alpha}{2}}} du\right)$$

$$\overset{(d)}{=} \exp\left(\frac{2\pi\lambda}{2-\alpha} \Gamma_{\mathrm{C}} r_{1,\mathrm{C}}^{\alpha} r_{2,\mathrm{C}}^{2-\alpha} \times {}_2F_1\left(1, 1-\frac{2}{\alpha}; 2-\frac{2}{\alpha}; -\Gamma_{\mathrm{C}}\left(\frac{r_{2,\mathrm{C}}}{r_{1,\mathrm{C}}}\right)^{-\alpha}\right)\right). \quad (7)$$

In (7), step (a) follows from the i.i.d. $g_{i,\mathrm{C}}$ with the independence of $g_{i,\mathrm{C}}$ from $\Phi$. Step (b) is obtained based on the definition of the PGFL for the PPP. The integration limits range from $r_{2,\mathrm{C}}$ to $\infty$, considering that the closest intercell interferer is at least at a distance $r_{2,\mathrm{C}}$. Step (c) is achieved by changing the variable, $u = (v/(r_{1,\mathrm{C}}\Gamma_{\mathrm{C}}^{1/\alpha}))^2$, that follows $\Gamma_{\mathrm{C}} = \frac{P_t T_{\mathrm{C}}}{P_{t,\mathrm{C}} - T_{\mathrm{C}} P_{t,\mathrm{NC}}}$. According to Lemma 1, step (d) in (7) is obtained by a simple variable replacement and algebraic operation.

Similarly, $\mathcal{L}_{I'_{\mathrm{C}}}\left(\frac{\beta P_t T_{\mathrm{C}}}{P_{t,\mathrm{C}} - T_{\mathrm{C}} P_{t,\mathrm{NC}}} r_{2,\mathrm{C}}^{\alpha}\right)$ can be calculated as

$$\mathcal{L}_{I'_{\mathrm{C}}}\left(\frac{\beta P_t T_{\mathrm{C}}}{P_{t,\mathrm{C}} - T_{\mathrm{C}} P_{t,\mathrm{NC}}} r_{2,\mathrm{C}}^{\alpha}\right)$$

$$= \mathbb{E}\left[\exp\left(-sI'_{\mathrm{C}}\right)\right]\Big|_{s=\frac{\beta P_t T_{\mathrm{C}}}{P_{t,\mathrm{C}} - T_{\mathrm{C}} P_{t,\mathrm{NC}}} r_{2,\mathrm{C}}^{\alpha}}$$

$$= \exp\left(-2\pi\lambda \int_{r_{2,\mathrm{C}}}^{\infty} \frac{\Gamma_{\mathrm{C}}}{\Gamma_{\mathrm{C}} + (v/r_{2,\mathrm{C}})^{\alpha}} v dv\right)\Bigg|_{\Gamma_{\mathrm{C}}=\frac{P_t T_{\mathrm{C}}}{P_{t,\mathrm{C}} - T_{\mathrm{C}} P_{t,\mathrm{NC}}}}$$

$$\overset{(a)}{=} \exp\left(-\pi\lambda r_{2,\mathrm{C}}^2 \Gamma_{\mathrm{C}}^{\frac{2}{\alpha}} \int_{\Gamma_{\mathrm{C}}^{-\frac{2}{\alpha}}}^{\infty} \frac{1}{1+u^{\frac{\alpha}{2}}} du\right)$$

$$= \exp\left(\frac{2\pi\lambda}{2-\alpha} \Gamma_{\mathrm{C}} r_{2,\mathrm{C}}^2 \cdot {}_2F_1\left(1, 1-\frac{2}{\alpha}; 2-\frac{2}{\alpha}; -\Gamma_{\mathrm{C}}\right)\right). \quad (8)$$

In (8), step (a) is based on changing the variable, $u = (v/(r_{2,\mathrm{C}}\Gamma_{\mathrm{C}}^{1/\alpha}))^2$, which is a noteworthy difference from (7).

Finally, the desired result of $\mathbb{P}[\mathrm{SINR}_{\mathrm{C}} > T_{\mathrm{C}}]$ can be derived by substituting (7) and (8) into (6). For simplicity, by performing variable substitution directly and a simple algebraic operation, the desired result of $\mathbb{P}[\mathrm{SINR}_{\mathrm{C}} > T_{\mathrm{C}}]$ can be rewritten as (9), shown at the bottom of the next page.

Recall that in the framework developed, the typical user can access wireless networks as a CoMP UE only when it is outside the Stienen disk. Accordingly, the coverage probability for the typical user, such as the typical CoMP UE $\mathcal{P}_{\mathrm{O}\to\mathrm{CoMP}}$, is a conditional probability. Consequently, considering Lemma 3 and (9), it yields (10), shown at the bottom of the next page.

### C. Coverage for the Typical Non-CoMP UE

In the system model of this study, when the typical user is served as a non-CoMP UE, it is called the typical non-CoMP UE. According to the joint JT-CoMP-NOMA scheme, the typical non-CoMP UE is included in a certain NOMA group, which comprises a CoMP UE at the same time. Obviously, the nearest BS for the typical non-CoMP UE is also the nearest BS for such CoMP UE. Then, the received signal at the typical non-CoMP UE can be identically represented as that at the non-CoMP UE inside the Stienen disk of BS1 in Fig. 2. A non-CoMP UE first decodes and subtracts the transmitted signal for a CoMP UE and then decodes its own desired signal without interference from the CoMP UE. Accordingly, two steps are performed. In the first step, the typical non-CoMP UE decodes $x_{1,\mathrm{C}}$ and removes it from the received composite signal. In the second step, the typical non-CoMP UE decodes $x_{1,\mathrm{NC}}$ from the remaining received composite signals. Based on (2), the SINRs in these two steps for the typical non-CoMP UE can be expressed as follows: i)

$$\mathrm{SINR}_{\mathrm{NC}}^{\mathrm{I}} = \frac{P_{t,\mathrm{C}} h_{1,\mathrm{NC}}}{P_{t,\mathrm{NC}} h_{1,\mathrm{NC}} + \sum_{i>1} P_t h_{i,\mathrm{NC}} + \sigma^2} \quad (11)$$

$$\mathbb{P}[\mathrm{SINR}_{\mathrm{C}} > T_{\mathrm{C}}] = \mathbb{E}\left[\frac{1}{A-B}\left(A\exp\left(-\frac{\beta}{A}C\right) - B\exp\left(-\frac{\beta}{B}C\right)\right)\right]$$

$$\overset{(a)}{=} \mathbb{E}\left[\frac{r_{2,\mathrm{C}}^{\alpha}}{r_{2,\mathrm{C}}^{\alpha} - r_{1,\mathrm{C}}^{\alpha}} \exp\left(-\frac{\beta\sigma^2 T_{\mathrm{C}}}{P_{t,\mathrm{C}} - T_{\mathrm{C}} P_{t,\mathrm{NC}}} r_{1,\mathrm{C}}^{\alpha}\right) \exp\left(-\frac{\beta P_t T_{\mathrm{C}}}{P_{t,\mathrm{C}} - T_{\mathrm{C}} P_{t,\mathrm{NC}}} r_{1,\mathrm{C}}^{\alpha} I'_{\mathrm{C}}\right)\right.$$
$$\left. - \frac{r_{1,\mathrm{C}}^{\alpha}}{r_{2,\mathrm{C}}^{\alpha} - r_{1,\mathrm{C}}^{\alpha}} \exp\left(-\frac{\beta\sigma^2 T_{\mathrm{C}}}{P_{t,\mathrm{C}} - T_{\mathrm{C}} P_{t,\mathrm{NC}}} r_{2,\mathrm{C}}^{\alpha}\right) \exp\left(-\frac{\beta P_t T_{\mathrm{C}}}{P_{t,\mathrm{C}} - T_{\mathrm{C}} P_{t,\mathrm{NC}}} r_{2,\mathrm{C}}^{\alpha} I'_{\mathrm{C}}\right)\right]$$

$$\overset{(b)}{\approx} \mathbb{E}\left[\frac{r_{2,\mathrm{C}}^{\alpha}}{r_{2,\mathrm{C}}^{\alpha} - r_{1,\mathrm{C}}^{\alpha}} \exp\left(-\frac{\beta\sigma^2 T_{\mathrm{C}}}{P_{t,\mathrm{C}} - T_{\mathrm{C}} P_{t,\mathrm{NC}}} r_{1,\mathrm{C}}^{\alpha}\right) \mathcal{L}_{I'_{\mathrm{C}}}\left(\frac{\beta P_t T_{\mathrm{C}}}{P_{t,\mathrm{C}} - T_{\mathrm{C}} P_{t,\mathrm{NC}}} r_{1,\mathrm{C}}^{\alpha}\right)\right.$$
$$\left. - \frac{r_{1,\mathrm{C}}^{\alpha}}{r_{2,\mathrm{C}}^{\alpha} - r_{1,\mathrm{C}}^{\alpha}} \exp\left(-\frac{\beta\sigma^2 T_{\mathrm{C}}}{P_{t,\mathrm{C}} - T_{\mathrm{C}} P_{t,\mathrm{NC}}} r_{2,\mathrm{C}}^{\alpha}\right) \mathcal{L}_{I'_{\mathrm{C}}}\left(\frac{\beta P_t T_{\mathrm{C}}}{P_{t,\mathrm{C}} - T_{\mathrm{C}} P_{t,\mathrm{NC}}} r_{2,\mathrm{C}}^{\alpha}\right)\right]$$

$$\overset{(c)}{=} \iiint_{V_{\mathrm{C}}=\{(x,y,z):0<z<x\le y\}} \left(\frac{y^{\alpha}}{y^{\alpha} - x^{\alpha}} \exp\left(-\frac{\beta\sigma^2 T_{\mathrm{C}}}{P_{t,\mathrm{C}} - T_{\mathrm{C}} P_{t,\mathrm{NC}}} x^{\alpha}\right) \mathcal{L}_{I'_{\mathrm{C}}}\left(\frac{\beta P_t T_{\mathrm{C}}}{P_{t,\mathrm{C}} - T_{\mathrm{C}} P_{t,\mathrm{NC}}} x^{\alpha}\right)\right.$$
$$\left. - \frac{x^{\alpha}}{y^{\alpha} - x^{\alpha}} \exp\left(-\frac{\beta\sigma^2 T_{\mathrm{C}}}{P_{t,\mathrm{C}} - T_{\mathrm{C}} P_{t,\mathrm{NC}}} y^{\alpha}\right) \mathcal{L}_{I'_{\mathrm{C}}}\left(\frac{\beta P_t T_{\mathrm{C}}}{P_{t,\mathrm{C}} - T_{\mathrm{C}} P_{t,\mathrm{NC}}} y^{\alpha}\right)\right) f_{(r_{1,\mathrm{C}}, r_{2,\mathrm{C}})}(x,y) f_{R_{\mathrm{S}}}(z) dz dx dy \quad (6)$$

in Step 1, and ii)

$$\mathrm{SINR}_{\mathrm{NC}}^{\mathrm{II}} = \frac{P_{t,\mathrm{NC}} h_{1,\mathrm{NC}}}{\sum\limits_{i>1} P_t h_{i,\mathrm{NC}} + \sigma^2} \tag{12}$$

in Step 2. $I_{\mathrm{NC}} = \sum\limits_{i>1} P_t h_{i,\mathrm{NC}} = \sum\limits_{i>1} P_t r_{i,\mathrm{NC}}^{-\alpha} g_{i,\mathrm{NC}}$ is the cumulative ICI from all other BSs (i.e., $\Phi$ excluding BS1) to the typical non-CoMP UE. Thus, considering the implementation of SIC, it would succeed in the coverage for the typical non-CoMP UE when both steps are taken easily. Let $T_{\mathrm{NC}}^{\mathrm{I}}$ and $T_{\mathrm{NC}}^{\mathrm{II}}$ denote the SINR thresholds in these two steps respectively. The coverage probability for the typical non-CoMP UE is derived as

$$\begin{aligned}
&\mathbb{P}\left[\mathrm{SINR}_{\mathrm{NC}}^{\mathrm{I}} > T_{\mathrm{NC}}^{\mathrm{I}}, \mathrm{SINR}_{\mathrm{NC}}^{\mathrm{II}} > T_{\mathrm{NC}}^{\mathrm{II}}\right] \\
&= \mathbb{P}\left[h_{1,\mathrm{NC}} > \frac{T_{\mathrm{NC}}^{\mathrm{I}}}{P_{t,\mathrm{C}} - T_{\mathrm{NC}}^{\mathrm{I}} P_{t,\mathrm{NC}}} \left(I_{\mathrm{NC}} + \sigma^2\right),\right. \\
&\quad \left. h_{1,\mathrm{NC}} > \frac{T_{\mathrm{NC}}^{\mathrm{II}}}{P_{t,\mathrm{NC}}} \left(I_{\mathrm{NC}} + \sigma^2\right)\right] \\
&= \mathbb{P}\left[h_{1,\mathrm{NC}} > T_{\mathrm{NC}}^{\mathrm{MAX}} \left(I_{\mathrm{NC}} + \sigma^2\right)\right],
\end{aligned} \tag{13}$$

where $T_{\mathrm{NC}}^{\mathrm{MAX}} = \max\left\{\frac{T_{\mathrm{NC}}^{\mathrm{I}}}{P_{t,\mathrm{C}} - T_{\mathrm{NC}}^{\mathrm{I}} P_{t,\mathrm{NC}}}, \frac{T_{\mathrm{NC}}^{\mathrm{II}}}{P_{t,\mathrm{NC}}}\right\}$. Moreover, because of the characteristics of Rayleigh fading,

$$\begin{aligned}
&\mathbb{P}\left[\mathrm{SINR}_{\mathrm{NC}}^{\mathrm{I}} > T_{\mathrm{NC}}^{\mathrm{I}}, \mathrm{SINR}_{\mathrm{NC}}^{\mathrm{II}} > T_{\mathrm{NC}}^{\mathrm{II}}\right] \\
&= \mathbb{P}\left[g_{1,\mathrm{NC}} > T_{\mathrm{NC}}^{\mathrm{MAX}} r_{1,\mathrm{NC}}^{\alpha} \left(I_{\mathrm{NC}} + \sigma^2\right)\right] \\
&= \mathbb{E}\left[\exp\left(-\beta T_{\mathrm{NC}}^{\mathrm{MAX}} r_{1,\mathrm{NC}}^{\alpha} \left(I_{\mathrm{NC}} + \sigma^2\right)\right)\right] \\
&= \mathbb{E}\left[\exp\left(-\beta T_{\mathrm{NC}}^{\mathrm{MAX}} r_{1,\mathrm{NC}}^{\alpha} I_{\mathrm{NC}}\right) \exp\left(-\beta T_{\mathrm{NC}}^{\mathrm{MAX}} r_{1,\mathrm{NC}}^{\alpha} \sigma^2\right)\right].
\end{aligned} \tag{14}$$

Taking the Laplace transform would lead to incorrect results for a non-CoMP UE. Herein, we explain this and provide a modified version.

The radius of the Stienen disk, is correlated to that of the closest neighbor as a pair. Specifically, the statistical correlation between paired center points is newly introduced compared to the original PPP. Let $\Theta$ denote a set composed of all Stienen disks. This statistical correlation is an endogenetic characteristic of $\Theta$. Considering the location of the typical user, two categories of methods can deal with the statistical correlation: i) In the first category, because the typical user is outside the Stienen disk, $\Theta$ is homogeneous for the typical user. Performance analysis in which the typical user is concerned can be directly conducted regardless of such statistical correlations in $\Theta$. ii) In the second category, because the typical user is inside the Stienen disk, $\Theta$ is inhomogeneous for the typical user. When performance analysis focuses on the typical user, Stienen disk, in which the typical user is located, should be considered alone. Moreover, owing to the statistical correlation in $\Theta$, the other Stienen disk, where the center is closest to that of Stienen disk containing the typical user, must be individually considered as well. After removing these two Stienen disks, the remaining $\Theta$ form a new set. Clearly, this new set is homogeneous for the typical user and can be dealt with using classical approaches for the PPP.

Fig. 3 shows a partial enlargement when the typical user is a non-CoMP UE.

For the typical non-CoMP UE, BS1 transmits the desired signal, whereas the remaining BSs in $\Phi$, i.e., BS-$i$ ($i > 1$) are regarded as interferers. Let $\mathrm{BS}_2$ denote the second-nearest BS for the typical non-CoMP UE. Let $\mathrm{BS}_*$ denote the closest neighbor of BS1 in Fig. 3. Significantly, $\mathrm{BS}_*$ and $\mathrm{BS}_2$ are not always the same, although in the example (i.e., one realization of $\Phi$) shown in Fig. 3, $\mathrm{BS}_*$ is the second-nearest BS for the typical user. According to the second category of methods, $\mathrm{BS}_*$ should be treated separately from all interference BSs. In practice, $I_{\mathrm{NC}}$ is rewritten as $I_{\mathrm{NC}} = P_t D^{-\alpha} g_{*,\mathrm{NC}} + \sum\limits_{i:\chi_i \in \Phi \setminus \{\mathrm{BS1}, \mathrm{BS}_*\}} P_t r_{i,\mathrm{NC}}^{-\alpha} g_{i,\mathrm{NC}}$, where $D$ is the distance between $\mathrm{BS}_*$ and the typical non-CoMP UE. $I'_{\mathrm{NC}} = \frac{I_{\mathrm{NC}}}{P_t} = D^{-\alpha} g_{*,\mathrm{NC}} + \sum\limits_{i:\chi_i \in \Phi \setminus \{\mathrm{BS1}, \mathrm{BS}_*\}} r_{i,\mathrm{NC}}^{-\alpha} g_{i,\mathrm{NC}}$

$$\begin{aligned}
&\mathbb{P}\left[\mathrm{SINR}_{\mathrm{C}} > T_{\mathrm{C}}\right] \\
&= 4(\pi\lambda)^3 \Delta^{-2} \int_0^{\infty} \int_0^{y} \int_0^{x} \left( \frac{y^{\alpha}}{y^{\alpha} - x^{\alpha}} \exp\left(-\frac{\beta\sigma^2 \Gamma_{\mathrm{C}}}{P_t} x^{\alpha}\right) \exp\left(\frac{2\pi\lambda}{2-\alpha} \Gamma_{\mathrm{C}} x^{\alpha} y^{2-\alpha} \cdot {}_2F_1\left(1, 1 - \frac{2}{\alpha}; 2 - \frac{2}{\alpha}; -\Gamma_{\mathrm{C}} \left(\frac{x}{y}\right)^{\alpha}\right)\right)\right. \\
&\quad \left. - \frac{x^{\alpha}}{y^{\alpha} - x^{\alpha}} \exp\left(-\frac{\beta\sigma^2 \Gamma_{\mathrm{C}}}{P_t} y^{\alpha}\right) \exp\left(\frac{2\pi\lambda}{2-\alpha} \Gamma_{\mathrm{C}} y^2 \cdot {}_2F_1\left(1, 1 - \frac{2}{\alpha}; 2 - \frac{2}{\alpha}; -\Gamma_{\mathrm{C}}\right)\right)\right) \exp \\
&\quad \times \left(-\pi\lambda \left(y^2 + \left(\frac{z}{\Delta}\right)^2\right)\right) zxydzdxdy
\end{aligned} \tag{9}$$

$$\begin{aligned}
&\mathcal{P}_{\mathrm{O}\to\mathrm{CoMP}} \\
&= \frac{\mathbb{P}\left[\mathrm{SINR}_{\mathrm{C}} > T_{\mathrm{C}}\right]}{\mathbb{P}\left[\text{Typical user outside Stienen disk}\right]} = \frac{1}{1 - \Delta^2} \mathbb{P}\left[\mathrm{SINR}_{\mathrm{C}} > T_{\mathrm{C}}\right] \\
&= \frac{4(\pi\lambda)^3}{\Delta^2 - \Delta^4} \int_0^{\infty} \int_0^{y} \int_0^{x} \left( \frac{y^{\alpha}}{y^{\alpha} - x^{\alpha}} \exp\left(\frac{2\pi\lambda}{2-\alpha} \Gamma_{\mathrm{C}} x^{\alpha} y^{2-\alpha} \cdot {}_2F_1\left(1, 1 - \frac{2}{\alpha}; 2 - \frac{2}{\alpha}; -\Gamma_{\mathrm{C}} \left(\frac{x}{y}\right)^{\alpha}\right) - \frac{\beta\sigma^2 \Gamma_{\mathrm{C}}}{P_t} x^{\alpha}\right)\right. \\
&\quad \left. - \frac{x^{\alpha}}{y^{\alpha} - x^{\alpha}} \exp\left(\frac{2\pi\lambda}{2-\alpha} \Gamma_{\mathrm{C}} y^2 \cdot {}_2F_1\left(1, 1 - \frac{2}{\alpha}; 2 - \frac{2}{\alpha}; -\Gamma_{\mathrm{C}}\right) - \frac{\beta\sigma^2 \Gamma_{\mathrm{C}}}{P_t} y^{\alpha}\right)\right) \exp\left(-\pi\lambda \left(y^2 + \left(\frac{z}{\Delta}\right)^2\right)\right) zxydzdxdy
\end{aligned} \tag{10}$$

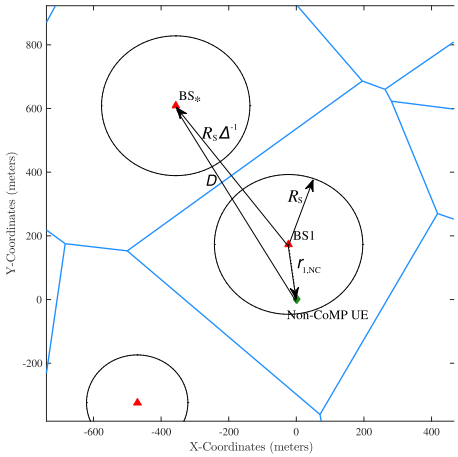


Fig. 3. Partial enlargement for explaining approximation when typical user is a non-CoMP UE.

indicates the normalized value of $I_{\mathrm{NC}}$. Thus, generally, the Laplace transform of $I_{\mathrm{NC}}$ is

$$\begin{aligned}
&\mathcal{L}_{I_{\mathrm{NC}}}\left(\beta T_{\mathrm{NC}}^{\mathrm{MAX}} r_{1,\mathrm{NC}}^{\alpha}\right)\\
&=\mathbb{E}\left[\exp\left(-\beta T_{\mathrm{NC}}^{\mathrm{MAX}} r_{1,\mathrm{NC}}^{\alpha} I_{\mathrm{NC}}\right)\right]\\
&=\mathbb{E}\left[\exp\left(-\beta P_t T_{\mathrm{NC}}^{\mathrm{MAX}} r_{1,\mathrm{NC}}^{\alpha} I'_{\mathrm{NC}}\right)\right]\\
&=\mathbb{E}\left[\exp\left(-sI'_{\mathrm{NC}}\right)\right]\Big|_{s=\beta P_t T_{\mathrm{NC}}^{\mathrm{MAX}} r_{1,\mathrm{NC}}^{\alpha}}\\
&=\mathbb{E}\left[\exp\left(-s\left(D^{-\alpha} g_{*,\mathrm{NC}}\right.\right.\right.\\
&\quad\left.\left.\left.+\sum_{i:\chi_i\in\Phi\setminus\{\mathrm{BS1},\mathrm{BS}_*\}} r_{i,\mathrm{NC}}^{-\alpha} g_{i,\mathrm{NC}}\right)\right)\right]\\
&=\mathbb{E}\left[\exp\left(-sD^{-\alpha} g_{*,\mathrm{NC}}\right)\right]\\
&\quad\times\mathbb{E}\left[\exp\left(-s\sum_{i:\chi_i\in\Phi\setminus\{\mathrm{BS1},\mathrm{BS}_*\}} r_{i,\mathrm{NC}}^{-\alpha} g_{i,\mathrm{NC}}\right)\right]. \qquad (15)
\end{aligned}$$

$\mathbb{E}\left[\exp\left(-\beta T_{\mathrm{NC}}^{\mathrm{MAX}} r_{1,\mathrm{NC}}^{\alpha} I_{\mathrm{NC}}\right)\right]$ is the product of two Laplace transforms. Considering $D$, the former can be further evaluated. For the latter, a derivation based on the definition of the PGFL for the PPP becomes applicable.

First, Fig. 3 shows that $D$ is the length of an edge of a triangle with vertices (i.e., BS$_*$, BS1, and non-CoMP UE). Let $\theta$ denote the angle between the edges of length $r_{1,\mathrm{NC}}$ and $R_{\mathrm{S}}\Delta^{-1}$. Based on the law of cosines, $D$ is obtained as $D=\sqrt{\left(R_{\mathrm{S}}\Delta^{-1}\right)^2+r_{1,\mathrm{NC}}^2-2R_{\mathrm{S}}\Delta^{-1}r_{1,\mathrm{NC}}\cos\left(\theta\right)}$. Considering that the position angle of the typical user is uniformly distributed [25], [29], $\theta$ is also uniformly distributed in $(0,\pi]$. The result of the integration for $D$ can then be given by

$$\begin{aligned}
\bar{D}&=\int_0^{\pi} D d\theta\\
&=\frac{2\left(R_{\mathrm{S}}\Delta^{-1}+r_{1,\mathrm{NC}}\right)}{\pi}\mathrm{EllipticE}\\
&\quad\times\left(\frac{\pi}{2},\frac{4R_{\mathrm{S}}\Delta^{-1}r_{1,\mathrm{NC}}}{\left(R_{\mathrm{S}}\Delta^{-1}+r_{1,\mathrm{NC}}\right)^2}\right), \qquad (16)
\end{aligned}$$

where $\mathrm{EllipticE}\left(\omega,k\right)$ [34, eq. (FI II 135)] denotes the elliptic integral of the second type, i.e., $\mathrm{EllipticE}\left(\omega,k\right)=\int_0^{\omega}\sqrt{1-k^2\sin^2 x}dx$. Using $\bar{D}$ as an approximation of $D$,[7] $\mathbb{E}\left[\exp\left(-sD^{-\alpha}g_{*,\mathrm{NC}}\right)\right]$ can be evaluated as follows:

$$\begin{aligned}
&\mathbb{E}\left[\exp\left(-sD^{-\alpha}g_{*,\mathrm{NC}}\right)\right]\Big|_{s=\beta P_t T_{\mathrm{NC}}^{\mathrm{MAX}} r_{1,\mathrm{NC}}^{\alpha}}\\
&\approx\mathbb{E}\left[\exp\left(-s\bar{D}^{-\alpha}g_{*,\mathrm{NC}}\right)\right]\\
&=\mathbb{E}\left[\exp\left(-\beta P_t T_{\mathrm{NC}}^{\mathrm{MAX}}\left(\frac{r_{1,\mathrm{NC}}}{\bar{D}}\right)^{\alpha} g_{*,\mathrm{NC}}\right)\right]\\
&=\left(1+P_t T_{\mathrm{NC}}^{\mathrm{MAX}}\left(\frac{r_{1,\mathrm{NC}}}{\bar{D}}\right)^{\alpha}\right)^{-1}, \qquad (17)
\end{aligned}$$

where the last step is obtained based on the PDF of $g_{*,\mathrm{NC}}$.

Second, as mentioned previously, set $\Phi\setminus\{\mathrm{BS1},\mathrm{BS}_*\}$ is homogeneous for the typical non-CoMP UE. Therefore,

$$\begin{aligned}
&\mathbb{E}\left[\exp\left(-s\sum_{i:\chi_i\in\Phi\setminus\{\mathrm{BS1},\mathrm{BS}_*\}} r_{i,\mathrm{NC}}^{-\alpha} g_{i,\mathrm{NC}}\right)\right]\\
&=\mathbb{E}\left[\prod_{i:\chi_i\in\Phi\setminus\{\mathrm{BS1},\mathrm{BS}_*\}}\mathbb{E}\left[\exp\left(-sr_{i,\mathrm{NC}}^{-\alpha}g\right)\right]\right]\\
&\overset{(a)}{\approx}\exp\left(-2\pi\lambda\int_{\bar{D}}^{\infty}\left(1-\mathbb{E}\left[\exp\left(-sv^{-\alpha}g\right)\right]\right)vdv\right)\\
&=\exp\left(-2\pi\lambda\int_{\bar{D}}^{\infty}\frac{\Gamma_{\mathrm{NC}}}{\Gamma_{\mathrm{NC}}+\left(v/r_{1,\mathrm{NC}}\right)^{\alpha}}vdv\right)\Big|_{\Gamma_{\mathrm{NC}}=P_t T_{\mathrm{NC}}^{\mathrm{MAX}}}\\
&\overset{(b)}{=}\exp\left(-\pi\lambda r_{1,\mathrm{NC}}^2\Gamma_{\mathrm{NC}}^{\frac{2}{\alpha}}\int_{\left(\frac{\bar{D}}{r_{1,\mathrm{NC}}}\right)^2\Gamma_{\mathrm{NC}}^{-\frac{2}{\alpha}}}^{\infty}\frac{1}{1+u^{\frac{\alpha}{2}}}du\right)\\
&\overset{(c)}{=}\exp\left(\frac{2\pi\lambda}{2-\alpha}\Gamma_{\mathrm{NC}}r_{1,\mathrm{NC}}^{\alpha}\bar{D}^{2-\alpha}\right.\\
&\quad\left.\times{}_2F_1\left(1,1-\frac{2}{\alpha};2-\frac{2}{\alpha};-\Gamma_{\mathrm{NC}}\left(\frac{\bar{D}}{r_{1,\mathrm{NC}}}\right)^{-\alpha}\right)\right). \qquad (18)
\end{aligned}$$

An approximation is that the lower limit of the integration is $\bar{D}$ in step (a) of (18). This can be explained by investigating the relationship between BS$_*$ and BS$_2$. Here, $r_{2,\mathrm{NC}}$ denotes the distance between BS$_2$ and the typical non-CoMP UE. When BS$_*$ and BS$_2$ are the same, the lower limit of the integration is $D$, considering that the closest intercell interferer in $\Phi\setminus\{\mathrm{BS1},\mathrm{BS}_*\}$ is at least at a distance $D$. When BS$_*$ is different from BS$_2$, the lower limit of the integration is $r_{2,\mathrm{NC}}$, considering that the closest intercell interferer in $\Phi\setminus\{\mathrm{BS1},\mathrm{BS}_*\}$ is at a distance $r_{2,\mathrm{NC}}$. With the acceptable (sometimes negligible) loss of numerical accuracy, the lower limit of the integration is uniformly set to $D$ regardless of the case. This approach is similar to those in [26] and [27]. Moreover, step (a) is achieved by substituting $\bar{D}$ for $D$. In (18), step (b) is obtained by changing the variables, $u=(v/(r_{1,\mathrm{NC}}\Gamma_{\mathrm{NC}}^{1/\alpha}))^2$, which follows up $\Gamma_{\mathrm{NC}}=P_t T_{\mathrm{NC}}^{\mathrm{MAX}}$. Based on Lemma 1, step (c) is obtained by a simple variable replacement and algebraic operation.

Finally, $\mathbb{P}\left[\mathrm{SINR}_{\mathrm{NC}}^{\mathrm{I}}>T_{\mathrm{NC}}^{\mathrm{I}},\mathrm{SINR}_{\mathrm{NC}}^{\mathrm{II}}>T_{\mathrm{NC}}^{\mathrm{II}}\right]$ is given as (19), as shown at the bottom of page 11. In step (a), the expectation is expressed as a double integral over the

[7]Note that $D\approx\sqrt{\left(R_{\mathrm{S}}\Delta^{-1}\right)^2+r_{1,\mathrm{NC}}^2}$ was used as an approximation of $D$ in [13], [26], and [27]. And $\theta$ was omitted in such approximation. Obviously, using $\bar{D}$ as an approximation of $D$ in this study is better in statistics, because $\bar{D}$ is the result of the integration for $D$ with the integral variable $\theta$.

region $V_{\mathrm{NC}}$. In step (b), by direct variable substitution $\bar{D} \to \mathrm{FuncD}\,(x,z)$ and simple algebraic operation, the desired result of $\mathbb{P}\left[\mathrm{SINR}_{\mathrm{NC}}^{\mathrm{I}} > T_{\mathrm{NC}}^{\mathrm{I}}, \mathrm{SINR}_{\mathrm{NC}}^{\mathrm{II}} > T_{\mathrm{NC}}^{\mathrm{II}}\right]$ is obtained with $\mathrm{FuncD}\,(x,z) = \frac{2}{\pi}\left(\Delta^{-1}z + x\right)\mathrm{EllipticE}\left(\frac{\pi}{2}, \frac{4\Delta^{-1}xz}{(\Delta^{-1}z+x)^2}\right)$.

It should be noted that in the system model, the typical user is a non-CoMP UE only when this UE is inside Stienen disk. Specifically, the coverage probability for the typical user as the typical non-CoMP UE, $\mathcal{P}_{\mathrm{O}\to\mathrm{Non-CoMP}}$, is the conditional probability. Finally, with Lemma 3 and (19), we obtain (20), shown at the bottom of the next page.

## IV. Average Achievable Rates

To evaluate the data rate over a cell, the average achievable rate is crucial for performance analysis. According to the definition[8] in [37], the average achievable rate is calculated as $\mathbb{E}\left[\ln\left(1+\mathrm{SINR}\right)\right]$, assuming that a UE can reach the Shannon bound for its instantaneous SINR. Specifically, both CoMP and non-CoMP UEs can always decode their own desired signals successfully. In this section, we derive the expressions of the average achievable rates of these two types of UEs.

### A. Data Rate for CoMP UE

Considering the system model of this study, the average achievable rate of the CoMP UEs is $\mathcal{R}_{\mathrm{CoMP}} = \mathbb{E}\left[\ln\left(1+\mathrm{SINR}_{\mathrm{C}}\right)\right]$, where $\mathrm{SINR}_{\mathrm{C}}$ is expressed in (3). For a positive random variable $X$, $\mathbb{E}\left[X\right] = \int_{t>0}\mathbb{P}\left[X>t\right]dt$. Hence, similar to (4), (5), and (6), it follows

$$\begin{aligned}&\mathbb{E}\left[\ln\left(1+\mathrm{SINR}_{\mathrm{C}}\right)\right]\\&= \iiint_{V_{\mathrm{C}}}\int_{t>0}\mathbb{P}\left[\left(\frac{P_{t,\mathrm{C}}-\left(e^t-1\right)P_{t,\mathrm{NC}}}{x^{\alpha}}g_{1,\mathrm{C}}\right.\right.\\&\left.\left.+\frac{P_{t,\mathrm{C}}-\left(e^t-1\right)P_{t,\mathrm{NC}}}{y^{\alpha}}g_{2,\mathrm{C}}\right) > \left(I_{\mathrm{C}}+\sigma^2\right)\left(e^t-1\right)\right]dt\\&\times f_{(r_{1,\mathrm{C}},r_{2,\mathrm{C}})}(x,y)f_{R_{\mathrm{S}}}(z)dzdxdy\,.\end{aligned}\tag{21}$$

An explicit expression similar to (9) can be obtained based on (21). It is in the form of a quadruple integral that, in theory, gives the precise value for specific parameters. However, it is difficult to integrate numerically. The numerical issues are caused by the existence of $e^t$ in the coefficients of $g_{1,\mathrm{C}}$ and $g_{2,\mathrm{C}}$.

For any $x,y,z\in\mathbb{R}^+$, $\ln\left(1+\frac{x}{y+z}\right) = \ln\left(1+\frac{x+y}{z}\right) - \ln\left(1+\frac{y}{z}\right)$. Using this property, $\ln\left(1+\mathrm{SINR}_{\mathrm{C}}\right)$ can be rewritten as

$$\begin{aligned}&\ln\left(1+\mathrm{SINR}_{\mathrm{C}}\right)\\&= \ln\left(1+\frac{P_t r_{1,\mathrm{C}}^{-\alpha}g_{1,\mathrm{C}}+P_t r_{2,\mathrm{C}}^{-\alpha}g_{2,\mathrm{C}}}{I_{\mathrm{C}}+\sigma^2}\right)\\&\quad-\ln\left(1+\frac{P_{t,\mathrm{NC}} r_{1,\mathrm{C}}^{-\alpha}g_{1,\mathrm{C}}+P_{t,\mathrm{NC}} r_{2,\mathrm{C}}^{-\alpha}g_{2,\mathrm{C}}}{I_{\mathrm{C}}+\sigma^2}\right),\end{aligned}\tag{22}$$

considering $P_t = P_{t,\mathrm{NC}} + P_{t,\mathrm{C}}$. Thus, $\mathcal{R}_{\mathrm{CoMP}}$ is given as

$$\begin{aligned}&\mathcal{R}_{\mathrm{CoMP}}\\&= \mathbb{E}\left[\ln\left(1+\mathrm{SINR}_{\mathrm{C}}\right)\right]\\&= \underbrace{\mathbb{E}\left[\ln\left(1+\frac{P_t r_{1,\mathrm{C}}^{-\alpha}g_{1,\mathrm{C}}+P_t r_{2,\mathrm{C}}^{-\alpha}g_{2,\mathrm{C}}}{I_{\mathrm{C}}+\sigma^2}\right)\right]}_{\text{Item 1}}\\&\quad\underbrace{-\mathbb{E}\left[\ln\left(1+\frac{P_{t,\mathrm{NC}} r_{1,\mathrm{C}}^{-\alpha}g_{1,\mathrm{C}}+P_{t,\mathrm{NC}} r_{2,\mathrm{C}}^{-\alpha}g_{2,\mathrm{C}}}{I_{\mathrm{C}}+\sigma^2}\right)\right]}_{\text{Item 2}}\\&= \mathcal{R}_{\mathrm{CoMP}}^{\mathrm{Item1}} - \mathcal{R}_{\mathrm{CoMP}}^{\mathrm{Item2}}\,.\end{aligned}\tag{23}$$

The average achievable rate of the CoMP UEs is obtained by successively calculating two items. For the first item, similar to (9), it follows (24), shown at the bottom of the next page, based on changing in variables $\rho = e^t - 1$. Similarly, the second item of the average achievable rate of the CoMP UEs can be calculated by (25), shown at the bottom of the next page. Finally, the average achievable rate of the CoMP UEs is derived using $\mathcal{R}_{\mathrm{CoMP}} = \mathcal{R}_{\mathrm{CoMP}}^{\mathrm{Item1}} - \mathcal{R}_{\mathrm{CoMP}}^{\mathrm{Item2}}$ based on (24) and (25).

### B. Data Rate for Non-CoMP UE

In the system model of this study, the average achievable rate of the non-CoMP UEs is $\mathcal{R}_{\mathrm{Non-CoMP}} = \mathbb{E}\left[\ln\left(1+\mathrm{SINR}_{\mathrm{NC}}^{\mathrm{II}}\right)\right]$, where $\mathrm{SINR}_{\mathrm{NC}}^{\mathrm{II}}$ is expressed in (12). It similarly follows from (15), (17), and (18) as described in Subsection III-C, and yields (26).

## V. Numerical Results and Discussions

In this section, we present numerically evaluated analytical and simulation results of the developed framework. The main system parameters in this study are similar to those in [6], [12], and [21]. Specifically, the path loss exponent is $\alpha = 3.5$. Rayleigh fading is normalized, i.e., $\beta = 1$. The channel bandwidth, $W$, is 10MHz. The AWGN power spectral density is $-174$dBm/Hz. Correspondingly, $\sigma^2 = 10^{-13.4}$W. A simulation area of $5\mathrm{km}\times 5\mathrm{km}$ is considered in the Monte Carlo simulations. The intensity of the UEs is $7\lambda$. Owing to the similarity between the procedures of decoding signals at a CoMP UE and the first step of a non-CoMP UE, without loss of generality, for the SINR thresholds, $T_{\mathrm{C}}$ and $T_{\mathrm{NC}}^{\mathrm{I}}$, the same $\gamma_o$ value is used [12].

### A. System Performance Versus Power Allocation Coefficient

In this subsection, macrocell networks are considered with a BS intensity of $\lambda = \left(500^2\pi\right)^{-1}$ and BS total transmission power of $P_t = 46$dBm. In addition, the SINR thresholds are set to $T_{\mathrm{C}} = T_{\mathrm{NC}}^{\mathrm{I}} = \gamma_o = 2$dB and $T_{\mathrm{NC}}^{\mathrm{II}} = 5$dB.

Fig. 4 shows the coverage probabilities of the typical CoMP and non-CoMP UEs, i.e., $\mathcal{P}_{\mathrm{O}\to\mathrm{CoMP}}$ and $\mathcal{P}_{\mathrm{O}\to\mathrm{Non-CoMP}}$, respectively, with varying $\epsilon$. First, it can be seen that the analytical results ("Anal." in Fig. 4) well match the simulation results ("Simul." in Fig. 4). A negligible difference is observed between the analytical and simulation results. This gap is caused by approximations in the derivations in Section III.

[8] $\mathbb{E}\left[\ln\left(1+\mathrm{SINR}\right)\right]$ is the spectral efficiency. Here we assume a normalized bandwidth, so we can interpret it as the average achievable rate, without loss of generality. This approach is widely adopted in the relevant literature, see, e.g., [6], [7], [12], [13], [16], [18], [19], [21], and [37].

Second, $\mathcal{P}_{\mathrm{O}\to\mathrm{CoMP}}$ decreases monotonically with increasing $\epsilon$. $\mathcal{P}_{\mathrm{O}\to\mathrm{Non-CoMP}}$ first increases and then decreases as $\epsilon$ increases. Moreover, both $\mathcal{P}_{\mathrm{O}\to\mathrm{CoMP}}$ and $\mathcal{P}_{\mathrm{O}\to\mathrm{Non-CoMP}}$ curves are truncated at $\epsilon = 0.39$. This can be interpreted in terms of the definition of $\epsilon$. Recall that $\epsilon$ is the power allocation coefficient for the near NOMA UEs. A large $\epsilon$ implies high power is allocated to the non-CoMP UEs, and low power is allocated to the CoMP UEs. Evidently, considering that a CoMP UE directly decodes its own desired signal in one step, the failure of decoding at a CoMP UE is more probable with low allocated power. However, to access wireless networks successfully, the non-CoMP UEs perform successively two

$$\begin{aligned}
&\mathbb{P}\left[\mathrm{SINR}_{\mathrm{NC}}^{\mathrm{I}} > T_{\mathrm{NC}}^{\mathrm{I}}, \mathrm{SINR}_{\mathrm{NC}}^{\mathrm{II}} > T_{\mathrm{NC}}^{\mathrm{II}}\right] = \mathbb{E}\left[\exp\left(-\beta T_{\mathrm{NC}}^{\mathrm{MAX}} r_{1,\mathrm{NC}}^{\alpha} I_{\mathrm{NC}}\right)\exp\left(-\beta T_{\mathrm{NC}}^{\mathrm{MAX}} r_{1,\mathrm{NC}}^{\alpha}\sigma^2\right)\right] \\
&\approx \mathbb{E}\left[\mathcal{L}_{I_{\mathrm{NC}}}\left(\beta T_{\mathrm{NC}}^{\mathrm{MAX}} r_{1,\mathrm{NC}}^{\alpha}\right)\exp\left(-\beta T_{\mathrm{NC}}^{\mathrm{MAX}} r_{1,\mathrm{NC}}^{\alpha}\sigma^2\right)\right] \\
&\overset{(a)}{=} \int\limits_{V_{\mathrm{NC}}=\{(x,z):0<x\le z\}} \exp\left(-\beta T_{\mathrm{NC}}^{\mathrm{MAX}} x^{\alpha}\sigma^2\right)\left(1+P_t T_{\mathrm{NC}}^{\mathrm{MAX}}\left(\frac{x}{\bar{D}}\right)^{\alpha}\right)^{-1} \\
&\quad\times \exp\left(\frac{2\pi\lambda}{2-\alpha}\Gamma_{\mathrm{NC}} x^{\alpha}\bar{D}^{2-\alpha}\cdot {}_2F_1\left(1,1-\frac{2}{\alpha};2-\frac{2}{\alpha};-\Gamma_{\mathrm{NC}}\left(\frac{\bar{D}}{x}\right)^{-\alpha}\right)\right) f_{r_{1,\mathrm{NC}}}(x) f_{R_{\mathrm{S}}}(z)\,dzdx \\
&\overset{(b)}{=} 4(\pi\lambda)^2\Delta^{-2}\int_0^{\infty}\int_0^{z}\left(1+\Gamma_{\mathrm{NC}}\left(\frac{x}{\mathrm{FuncD}\,(x,z)}\right)^{\alpha}\right)^{-1}\exp\left(-\frac{\beta\sigma^2\Gamma_{\mathrm{NC}}}{P_t}x^{\alpha}-\pi\lambda\left(x^2+\left(\frac{z}{\Delta}\right)^2\right)\right) \\
&\quad\times \exp\left(\frac{2\pi\lambda}{2-\alpha}\Gamma_{\mathrm{NC}} x^{\alpha}(\mathrm{FuncD}\,(x,z))^{2-\alpha}\cdot {}_2F_1\left(1,1-\frac{2}{\alpha};2-\frac{2}{\alpha};-\Gamma_{\mathrm{NC}}\left(\frac{\mathrm{FuncD}\,(x,z)}{x}\right)^{-\alpha}\right)\right) xz\,dxdz
\end{aligned} \tag{19}$$

$$\begin{aligned}
\mathcal{P}_{\mathrm{O}\to\mathrm{Non-CoMP}} &= \frac{\mathbb{P}\left[\mathrm{SINR}_{\mathrm{NC}}^{\mathrm{I}} > T_{\mathrm{NC}}^{\mathrm{I}}, \mathrm{SINR}_{\mathrm{NC}}^{\mathrm{II}} > T_{\mathrm{NC}}^{\mathrm{II}}\right]}{\mathbb{P}\left[\text{Typical user inside Stienen disk}\right]} = \frac{1}{\Delta^2}\mathbb{P}\left[\mathrm{SINR}_{\mathrm{NC}}^{\mathrm{I}} > T_{\mathrm{NC}}^{\mathrm{I}}, \mathrm{SINR}_{\mathrm{NC}}^{\mathrm{II}} > T_{\mathrm{NC}}^{\mathrm{II}}\right] \\
&= 4(\pi\lambda)^2\Delta^{-4}\int_0^{\infty}\int_0^{z}\left(1+\Gamma_{\mathrm{NC}}\left(\frac{x}{\mathrm{FuncD}\,(x,z)}\right)^{\alpha}\right)^{-1}\exp\left(-\frac{\beta\sigma^2\Gamma_{\mathrm{NC}}}{P_t}x^{\alpha}-\pi\lambda\left(x^2+\left(\frac{z}{\Delta}\right)^2\right)\right) \\
&\quad\times \exp\left(\frac{2\pi\lambda}{2-\alpha}\Gamma_{\mathrm{NC}} x^{\alpha}(\mathrm{FuncD}\,(x,z))^{2-\alpha}\cdot {}_2F_1\left(1,1-\frac{2}{\alpha};2-\frac{2}{\alpha};-\Gamma_{\mathrm{NC}}\left(\frac{\mathrm{FuncD}\,(x,z)}{x}\right)^{-\alpha}\right)\right) xz\,dxdz
\end{aligned} \tag{20}$$

$$\begin{aligned}
&\mathcal{R}_{\mathrm{CoMP}}^{\mathrm{Item1}} \\
&= 4(\pi\lambda)^3\Delta^{-2}\int_0^{\infty}\int_0^{\infty}\int_0^{y}\int_0^{x}\left(\frac{y^{\alpha}}{y^{\alpha}-x^{\alpha}}\exp\left(\frac{2\pi\lambda}{2-\alpha}\rho x^{\alpha}y^{2-\alpha}\cdot {}_2F_1\left(1,1-\frac{2}{\alpha};2-\frac{2}{\alpha};-\rho\left(\frac{x}{y}\right)^{\alpha}\right)-\frac{\beta\sigma^2\rho}{P_t}x^{\alpha}\right)\right. \\
&\quad\left.-\frac{x^{\alpha}}{y^{\alpha}-x^{\alpha}}\exp\left(\frac{2\pi\lambda}{2-\alpha}\rho y^2\cdot {}_2F_1\left(1,1-\frac{2}{\alpha};2-\frac{2}{\alpha};-\rho\right)-\frac{\beta\sigma^2\rho}{P_t}y^{\alpha}\right)\right)\exp\left(-\pi\lambda\left(y^2+\left(\frac{z}{\Delta}\right)^2\right)\right)\frac{zxy}{\rho+1}dzdxdyd\rho
\end{aligned} \tag{24}$$

$$\begin{aligned}
&\mathcal{R}_{\mathrm{CoMP}}^{\mathrm{Item2}} \\
&= 4(\pi\lambda)^3\Delta^{-2}\int_0^{\infty}\int_0^{\infty}\int_0^{y}\int_0^{x}\left(\frac{y^{\alpha}}{y^{\alpha}-x^{\alpha}}\exp\left(\frac{2\pi\lambda}{2-\alpha}\cdot\frac{\rho}{\epsilon}x^{\alpha}y^{2-\alpha}\cdot {}_2F_1\left(1,1-\frac{2}{\alpha};2-\frac{2}{\alpha};-\frac{\rho}{\epsilon}\left(\frac{x}{y}\right)^{\alpha}\right)-\frac{\beta\sigma^2\rho}{P_{t,\mathrm{NC}}}x^{\alpha}\right)\right. \\
&\quad\left.-\frac{x^{\alpha}}{y^{\alpha}-x^{\alpha}}\exp\left(\frac{2\pi\lambda}{2-\alpha}\cdot\frac{\rho}{\epsilon}y^2\cdot {}_2F_1\left(1,1-\frac{2}{\alpha};2-\frac{2}{\alpha};-\frac{\rho}{\epsilon}\right)-\frac{\beta\sigma^2\rho}{P_{t,\mathrm{NC}}}y^{\alpha}\right)\right)\exp\left(-\pi\lambda\left(y^2+\left(\frac{z}{\Delta}\right)^2\right)\right)\frac{zxy}{\rho+1}dzdxdyd\rho
\end{aligned} \tag{25}$$

$$\begin{aligned}
&\mathcal{R}_{\mathrm{Non-CoMP}} \\
&= 4(\pi\lambda)^2\Delta^{-2}\int_0^{\infty}\int_0^{\infty}\int_0^{z}\left(1+\frac{\rho}{\epsilon}\left(\frac{x}{\mathrm{FuncD}\,(x,z)}\right)^{\alpha}\right)^{-1}\exp\left(-\frac{\beta}{P_{t,\mathrm{NC}}}\rho\sigma^2x^{\alpha}-\pi\lambda\left(x^2+\left(\frac{z}{\Delta}\right)^2\right)\right) \\
&\quad\times\exp\left(\frac{2\pi\lambda}{2-\alpha}\cdot\frac{\rho}{\epsilon}x^{\alpha}(\mathrm{FuncD}\,(x,z))^{2-\alpha}\cdot {}_2F_1\left(1,1-\frac{2}{\alpha};2-\frac{2}{\alpha};-\frac{\rho}{\epsilon}\left(\frac{x}{\mathrm{FuncD}\,(x,z)}\right)^{\alpha}\right)\right)\frac{xz}{\rho+1}dxdzd\rho
\end{aligned} \tag{26}$$

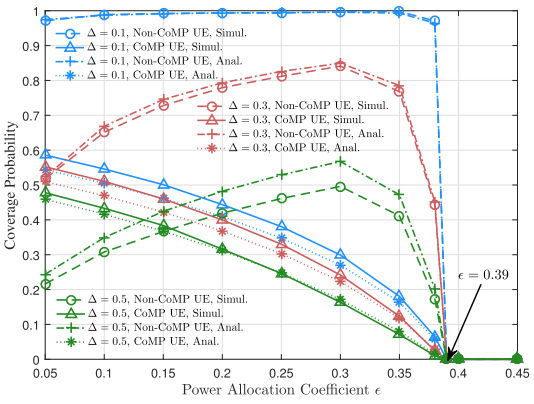


Fig. 4. Coverage probabilities of CoMP and non-CoMP UEs versus power allocation coefficient with different $\Delta$.

different steps of decoding signals. When $\epsilon$ increases, the low power allocated to a CoMP UE reduces the probability of successful decoding in the first step. Concurrently, the high power allocated to a non-CoMP UE increases the probability of successful decoding in the second step. This eventually leads to the nonmonotonic relationship between $\mathcal{P}_{\mathrm{O}\to\mathrm{Non-CoMP}}$ and $\epsilon$. In addition, the similarity between $\mathrm{SINR_C}$ and $\mathrm{SINR}_{\mathrm{NC}}^{\mathrm{I}}$ and between $T_{\mathrm{C}}$ and $T_{\mathrm{NC}}^{\mathrm{I}}$ result in identical truncations of the $\mathcal{P}_{\mathrm{O}\to\mathrm{CoMP}}$ and $\mathcal{P}_{\mathrm{O}\to\mathrm{Non-CoMP}}$ curves.

Fig. 5 depicts the average achievable rates of the CoMP and non-CoMP UEs with varying $\epsilon$ values. Recall that Section IV describes that the average achievable rate is calculated as $\mathbb{E}\left[\ln\left(1+\mathrm{SINR}\right)\right]$ in nats/Hz. Nevertheless, in practice, the data rate is typically measured in bits/Hz. For consistency with practice, we further utilize $\frac{W\mathcal{R}_{\mathrm{CoMP}}}{\ln 2}$ and $\frac{W\mathcal{R}_{\mathrm{Non-CoMP}}}{\ln 2}$ for the CoMP and non-CoMP UEs, respectively, in bits/Hz units, when the average achievable rate is analytically evaluated. First, Fig. 5 shows that the analytical results are very similar to the results obtained from the simulations. The negligible gap between the analytical and simulation results is due to approximations in the derivations presented in Section VI.

Second, the average achievable rates of the CoMP and non-CoMP UEs decrease and increase as $\epsilon$ increases, respectively. In terms of $\epsilon$, more transmission power allocation to a non-CoMP UE implies less power allocation to a CoMP UE. Thus, for the non-CoMP and CoMP UEs, decoding their own desired signals separately becomes easier and more difficult, respectively. In addition, interestingly, the relationship between the average achievable rate of the non-CoMP UEs and $\epsilon$ is monotonic, which is different from the nonmonotonic relationship between $\mathcal{P}_{\mathrm{O}\to\mathrm{Non-CoMP}}$ and $\epsilon$. This is because at the non-CoMP UEs, the data rate is only determined by the second step, whereas $\mathcal{P}_{\mathrm{O}\to\mathrm{Non-CoMP}}$ is simultaneously related to the two steps, as mentioned previously.

### B. Coverage Probability Versus SINR Threshold

In this subsection, the system performance versus the SINR threshold with different $\Delta$ is discussed. The average achievable rate is unaffected by the SINR threshold. Therefore, only the coverage probability is provided. Macrocell networks are considered with a BS intensity of $\lambda = \left(500^2\pi\right)^{-1}$ and BS total transmission power of $P_t = 46\mathrm{dBm}$. The power allocation coefficient is set to $\epsilon = 0.15$. In addition, the SINR thresholds

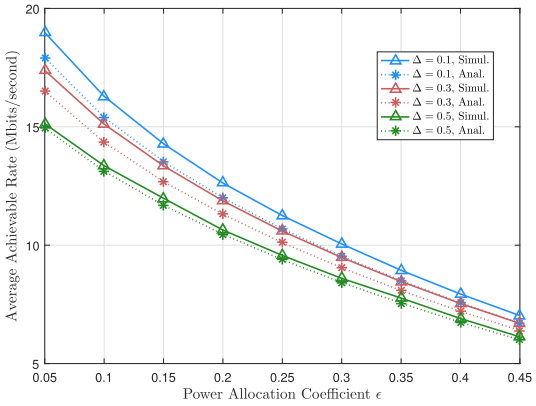


(a)

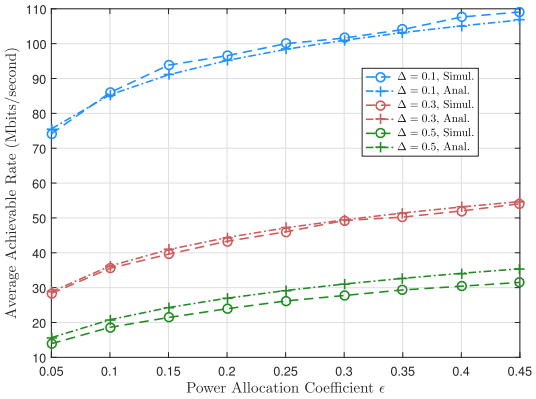


(b)

Fig. 5. Average achievable rates versus power allocation coefficient with different $\Delta$. (a) CoMP UE. (b) Non-CoMP UE.

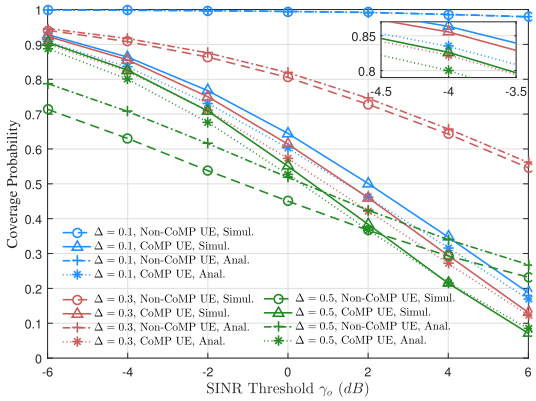


Fig. 6. Coverage probabilities of CoMP and non-CoMP UEs versus SINR threshold $\gamma_o$ with different $\Delta$.

are assumed to satisfy $T_{\mathrm{C}} = T_{\mathrm{NC}}^{\mathrm{I}} = \gamma_o$ and $T_{\mathrm{NC}}^{\mathrm{II}} - \gamma_o = 3\mathrm{dB}$ [12].

Fig. 6 presents the coverage probabilities of the typical CoMP and non-CoMP UEs, i.e., $\mathcal{P}_{\mathrm{O}\to\mathrm{CoMP}}$ and $\mathcal{P}_{\mathrm{O}\to\mathrm{Non-CoMP}}$ curves versus different $\gamma_o$ values. The figure shows that first, the accuracy of the derived expressions of $\mathcal{P}_{\mathrm{O}\to\mathrm{CoMP}}$ and $\mathcal{P}_{\mathrm{O}\to\mathrm{Non-CoMP}}$ is validated by a close match between the analytical and simulation results.

Second, as expected, both $\mathcal{P}_{\mathrm{O}\to\mathrm{CoMP}}$ and $\mathcal{P}_{\mathrm{O}\to\mathrm{Non-CoMP}}$ decrease monotonically as $\gamma_o$ increases. In Fig. 6, the decrease in $\mathcal{P}_{\mathrm{O}\to\mathrm{CoMP}}$ is greater than that in $\mathcal{P}_{\mathrm{O}\to\mathrm{Non-CoMP}}$ with the increase in $\gamma_o$ from $-6$dB to 6dB. Specifically, in terms of the coverage probabilities, the CoMP UEs are more sensitive to

the fluctuations in SINR thresholds than the non-CoMP UEs. This is understandable because the CoMP UEs in the proposed joint JT-CoMP-NOMA scheme are closer to the cell edge and thus suffer from poorer wireless communication environment than the non-CoMP UEs.

### C. Comparison of Different Transmission Schemes

Here we utilize the analytical results of this investigation and those two studies [6], [12], and compare the coverage probabilities and average achievable rates of three different transmission schemes: NOMA, JT-CoMP, and JT-CoMP-NOMA. For consistent comparison, microcell networks are considered with a BS intensity of $\lambda = \left(100^2\pi\right)^{-1}$ and a BS total transmission power of $P_t = 30\text{dBm}$. Noise is neglected, i.e., $\sigma^2 = 0\text{W}$. The SINR thresholds are set as $T_{\text{C}} = T_{\text{NC}}^{\text{I}} = \gamma_o = -2\text{dB}$ and $T_{\text{NC}}^{\text{II}} = 1\text{dB}$. The scalar factor $\Delta$ is 0.3.

In [12], two types of user pairing are used for the NOMA scheme: random pairing (RP) and selective pairing (SP). Cell-edge and cell-center UEs (EUs and CUs, respectively) are allowed to form a NOMA group. In our joint JT-CoMP-NOMA scheme, one EU is equivalent to a CoMP UE and one CU is called a non-CoMP UE. In [6], in the JT-CoMP scheme, multiple UEs are accommodated by OMA resource allocation. The performance was analyzed for the typical user without distinction between EUs and CUs. However, for a reasonable comparison, a UE with an SINR threshold -2dB($= T_{\text{C}} = T_{\text{NC}}^{\text{I}} = \gamma_o$) is still deemed to be one EU for the JT-CoMP scheme. A UE with an SINR threshold of 1dB($= T_{\text{NC}}^{\text{II}}$) is deemed to be one CU when the JT-CoMP scheme ("(OMA) CoMP" in Fig. 7) is considered.

Fig. 7a shows the variations of the coverage probabilities versus $\epsilon$. For a CU, the values of the coverage probability from JT-CoMP-NOMA are the largest. For an EU, JT-CoMP-NOMA is ranked second. In addition, from $\epsilon = 0.05$ to $\epsilon = 0.40$, the degree to which the coverage probability of a CU in the JT-CoMP-NOMA scheme is greater than that in the JT-CoMP scheme, is more than the degree to which the coverage probability of an EU in the JT-CoMP-NOMA scheme is smaller than that in the JT-CoMP scheme. Even though the former is smaller than the latter at $\epsilon = 0.45$, the difference is $-0.108$, which is tiny. In conclusion, in terms of coverage from the perspective of the entire system, the JT-CoMP-NOMA scheme outperforms the other schemes.

Fig. 7b presents the average achievable rates versus $\epsilon$. Because the average achievable rate is unrelated to the SINR threshold, the average achievable rates of the CU and EU are identical in the JT-CoMP scheme. In Fig. 7b, for a CU, the values of the average achievable rate in JT-CoMP-NOMA are the largest. For an EU, JT-CoMP-NOMA is ranked third. Significantly, although for an EU, the average achievable rate in the NOMA with SP scheme is typically greater than that in the JT-CoMP-NOMA scheme, we would not consider the NOMA with SP scheme next because of the corresponding coverage probability of zero. In Fig. 7b, from $\epsilon = 0.10$ to $\epsilon = 0.45$, the degree to which the average achievable rate of an CU in the JT-CoMP-NOMA scheme is greater than that in the JT-CoMP scheme, exceeds the degree to which the average achievable rate of an EU in the JT-CoMP-NOMA scheme is smaller than that in the JT-CoMP scheme. Even though the former becomes less than the latter at $\epsilon = 0.05$, the difference value is $-3.53$ and negligible on the order of the average achievable rate. Consequently, in terms of data rate from the perspective of the entire system, the JT-CoMP-NOMA scheme provides the best performance among the abovementioned schemes.

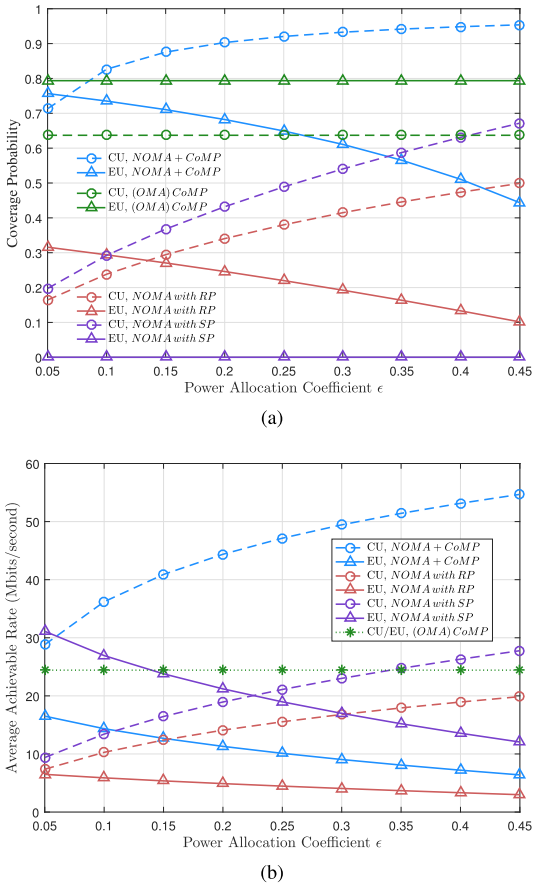


Fig. 7. Performances obtained with various schemes. (a) Coverage probabilities. (b) Average achievable rates.

## VI. Conclusion

In this study, we investigated a joint NOMA and JT-CoMP technique in a downlink network. A theoretical framework to analyze the system performance was developed based on stochastic geometry. Furthermore, the generalized Stienen model was used to divide the far and near NOMA UEs clearly, and to derive the analytical results of the coverage probability and average achievable rate for both CoMP and non-CoMP UEs. It was verified that the approximations in the derivations of expressions are tight by extensive comparisons between analytical results and Monte Carlo simulations. In addition, the effects of certain network parameters, such as the power allocation coefficient and a scalar factor $\Delta$, on the system performance were shown. It numerically revealed that the developed transmission scheme outperforms the NOMA-only and the JT-CoMP-only schemes in terms of the performance gain of the overall system.

Based on the research undertaken, analytically optimizing the power allocation coefficients to maximize the network spectral and energy efficiencies is one interesting topic for

future studies. Here we take the energy efficiency as an example and give a brief illustration. Based on (23) and (26) in this work, the formula of energy efficiency could be obtained further for a joint NOMA and JT-CoMP system. Differently from the typical expression of energy efficiency in [32] and [38], this formula would contain some integrals. In consequence, firstly we could utilize the numerical integration method to rewrite the formula into the series expansion form. Then, similarly to [32] and [38], the successive convex approximation and parameter transformation would be exploited to reduce the complexity in the optimization problem. Finally an iterative algorithm for power allocation could be designed.

Besides, extending the proposed framework to other advanced multiple access techniques and strategies for 6G wireless networks, merits the follow-up research too. In comparison to NOMA, rate-splitting multiple access (RSMA) has been recognized as another new paradigm for multiple access in 6G networks recently [39]. The architecture of RSMA in the physical layer is Multiple-Input Single-Output (MISO) or Multiple-Input Multiple-Output (MIMO), which is different from Single-Input Single-Output (SISO) adopted in the developed framework. Accordingly, if the current analysis method in this work is extended to RSMA or joint JT-CoMP-RSMA systems, the required (and complicated) adjustment of the SINR for each user needs to be carried out, specifically tailored to the Stienen model.

## REFERENCES


[1] W. Tong and P. Zhu, Eds., *6G: The Next Horizon: From Connected People and Things to Connected Intelligence*. Cambridge, U.K.: Cambridge Univ. Press, 2021.

[2] C.-X. Wang et al., "On the road to 6G: Visions, requirements, key technologies, and testbeds," *IEEE Commun. Surveys Tuts.*, vol. 25, no. 2, pp. 905–974, 2nd Quart. 2023.

[3] M. Chafii, L. Bariah, S. Muhaidat, and M. Debbah, "Twelve scientific challenges for 6G: Rethinking the foundations of communications theory," *IEEE Commun. Surveys Tuts.*, vol. 25, no. 2, pp. 868–904, 2nd Quart., 2023.

[4] *Coordinated Multi-Point Operation for LTE Physical Layer Aspects*, document TR 36.819, 3GPP, Sep. 2013.

[5] S. Bassoy, H. Farooq, M. A. Imran, and A. Imran, "Coordinated multi-point clustering schemes: A survey," *IEEE Commun. Surveys Tuts.*, vol. 19, no. 2, pp. 743–764, 2nd Quart., 2017.

[6] V. Garcia, Y. Zhou, and J. Shi, "Coordinated multipoint transmission in dense cellular networks with user-centric adaptive clustering," *IEEE Trans. Wireless Commun.*, vol. 13, no. 8, pp. 4297–4308, Aug. 2014.

[7] G. Nigam, P. Minero, and M. Haenggi, "Coordinated multipoint joint transmission in heterogeneous networks," *IEEE Trans. Commun.*, vol. 62, no. 11, pp. 4134–4146, Nov. 2014.

[8] M. Vaezi, Z. Ding, and H. V. Poor, *Multiple Access Techniques for 5G Wireless Networks and Beyond*. Cham, Switzerland: Springer, 2019.

[9] L. Dai, B. Wang, Z. Ding, Z. Wang, S. Chen, and L. Hanzo, "A survey of non-orthogonal multiple access for 5G," *IEEE Commun. Surveys Tuts.*, vol. 20, no. 3, pp. 2294–2323, 3rd Quart., 2018.

[10] Y. Liu et al., "Evolution of NOMA toward next generation multiple access (NGMA) for 6G," *IEEE J. Sel. Areas Commun.*, vol. 40, no. 4, pp. 1037–1071, Apr. 2022.

[11] Z. Ding, Z. Yang, P. Fan, and H. V. Poor, "On the performance of non-orthogonal multiple access in 5G systems with randomly deployed users," *IEEE Signal Process. Lett.*, vol. 21, no. 12, pp. 1501–1505, Dec. 2014.

[12] Z. Zhang, H. Sun, and R. Q. Hu, "Downlink and uplink non-orthogonal multiple access in a dense wireless network," *IEEE J. Sel. Areas Commun.*, vol. 35, no. 12, pp. 2771–2784, Dec. 2017.

[13] K. S. Ali, M. Haenggi, H. ElSawy, A. Chaaban, and M. Alouini, "Downlink non-orthogonal multiple access (NOMA) in Poisson networks," *IEEE Trans. Commun.*, vol. 67, no. 2, pp. 1613–1628, Feb. 2019.

[14] M. S. Ali, E. Hossain, and D. I. Kim, "Coordinated multipoint transmission in downlink multi-cell NOMA systems: Models and spectral efficiency performance," *IEEE Wireless Commun.*, vol. 25, no. 2, pp. 24–31, Apr. 2018.

[15] Y. Tian, A. R. Nix, and M. Beach, "On the performance of opportunistic NOMA in downlink CoMP networks," *IEEE Commun. Lett.*, vol. 20, no. 5, pp. 998–1001, May 2016.

[16] M. Elhattab, M. A. Arfaoui, and C. Assi, "A joint CoMP C-NOMA for enhanced cellular system performance," *IEEE Commun. Lett.*, vol. 24, no. 9, pp. 1919–1923, Sep. 2020.

[17] Y. Sun, Z. Ding, X. Dai, and G. K. Karagiannidis, "A feasibility study on network NOMA," *IEEE Trans. Commun.*, vol. 66, no. 9, pp. 4303–4317, Sep. 2018.

[18] Y. Sun, Z. Ding, X. Dai, M. Zhou, and Z. Ding, "Stochastic geometry based modeling and analysis on network NOMA in downlink CoMP systems," *IEEE Trans. Veh. Technol.*, vol. 73, no. 1, pp. 1388–1393, Jan. 2024.

[19] Y. Sun, Z. Ding, X. Dai, and O. A. Dobre, "On the performance of network NOMA in uplink CoMP systems: A stochastic geometry approach," *IEEE Trans. Commun.*, vol. 67, no. 7, pp. 5084–5098, Jul. 2019.

[20] Y. Tian, A. Nix, and M. Beach, "On the performance of a multi-tier NOMA strategy in coordinated multi-point networks," *IEEE Commun. Lett.*, vol. 21, no. 11, pp. 2448–2451, Nov. 2017.

[21] M. Elhattab, M.-A. Arfaoui, and C. Assi, "CoMP transmission in downlink NOMA-based heterogeneous cloud radio access networks," *IEEE Trans. Commun.*, vol. 68, no. 12, pp. 7779–7794, Dec. 2020.

[22] M. Elhattab, M. A. Arfaoui, and C. Assi, "Joint clustering and power allocation in coordinated multipoint assisted C-NOMA cellular networks," *IEEE Trans. Commun.*, vol. 70, no. 5, pp. 3483–3498, May 2022.

[23] Y. Dai, L. Lyu, and N. Cheng, "Impact of decoding order on user pairing in NOMA-CoMP joint transmission," *IEEE Trans. Veh. Technol.*, vol. 72, no. 7, pp. 9664–9669, Jul. 2023.

[24] Y. Sun, Z. Ding, X. Dai, M. Zhou, and Z. Ding, "On the application of quasi-degradation to network NOMA in downlink CoMP systems," *IEEE Trans. Wireless Commun.*, vol. 23, no. 2, pp. 978–993, Feb. 2024.

[25] S. Chiu, D. Stoyan, W. Kendall, and J. Mecke, *Stochastic Geometry and Its Applications*, 3rd ed., Hoboken, NJ, USA: Wiley, 2013.

[26] R. Hernandez-Aquino, S. A. R. Zaidi, M. Ghogho, D. McLernon, and A. Swami, "Stochastic geometric modeling and analysis of non-uniform two-tier networks: A Stienen's model-based approach," *IEEE Trans. Wireless Commun.*, vol. 16, no. 6, pp. 3476–3491, Jun. 2017.

[27] Z. H. Abbas, M. S. Haroon, F. Muhammad, G. Abbas, and F. Y. Li, "Enabling soft frequency reuse and Stienen's cell partition in two-tier heterogeneous networks: Cell deployment and coverage analysis," *IEEE Trans. Veh. Technol.*, vol. 70, no. 1, pp. 613–626, Jan. 2021.

[28] X. Yu, Q. Cui, and M. Haenggi, "Coherent joint transmission in downlink heterogeneous cellular networks," *IEEE Wireless Commun. Lett.*, vol. 7, no. 2, pp. 274–277, Apr. 2018.

[29] M. Haenggi, *Stochastic Geometry for Wireless Networks*. Cambridge, U.K.: Cambridge Univ. Press, 2012.

[30] *Study on Non-Orthogonal Multiple Access (NOMA) for NR (release 16)*, document TR 38.812, 3GPP, Dec. 2018.

[31] L. Lei, D. Yuan, C. K. Ho, and S. Sun, "Power and channel allocation for non-orthogonal multiple access in 5G systems: Tractability and computation," *IEEE Trans. Wireless Commun.*, vol. 15, no. 12, pp. 8580–8594, Dec. 2016.

[32] F. Fang, H. Zhang, J. Cheng, and V. C. M. Leung, "Energy-efficient resource allocation for downlink non-orthogonal multiple access network," *IEEE Trans. Commun.*, vol. 64, no. 9, pp. 3722–3732, Sep. 2016.

[33] Y. Chen, Q. Zhu, C. Feng, and X. Li, "Analysis of backlog and delay in downlink power-domain non-orthogonal multiple access wireless networks," *Comput. Commun.*, vol. 166, pp. 26–39, Jan. 2021.

[34] I. S. Gradshteyn and I. M. Ryzhik, *Table of Integrals, Series, and Products*, 6th ed., New York, NY, USA: Academic, 2000.

[35] D. Moltchanov, "Distance distributions in random networks," *Ad Hoc Netw.*, vol. 10, no. 6, pp. 1146–1166, Aug. 2012.

[36] M. Månsson, "A connection between the volume fractions of the stienen model and the dead leaves model," *Adv. Appl. Probab.*, vol. 39, no. 1, pp. 41–52, Mar. 2007.

[37] J. G. Andrews et al., "A tractable approach to coverage and rate in cellular networks," *IEEE Trans. Commun.*, vol. 59, no. 11, pp. 3122–3134, Nov. 2011.

[38] Y. Chen, Q. Zhu, C. Guo, Y. Yuan, and C. Feng, "Joint throughput-optimal scheduling and energy efficiency optimization for NOMA systems with flow-level dynamics," *IEEE Trans. Veh. Technol.*, vol. 72, no. 12, pp. 16667–16682, Dec. 2023.

[39] B. Clerckx et al., "Multiple access techniques for intelligent and multifunctional 6G: Tutorial, survey, and outlook," *Proc. IEEE*, vol. 112, no. 7, pp. 832–879, Jul. 2024.

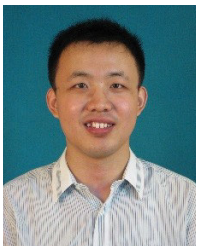

**Yunpei Chen** received the B.S. degree in communications engineering from Nanjing University of Posts and Telecommunications (NUPT), Nanjing, China, in 2006, the M.S. degree in communication and information systems from Beijing University of Posts and Telecommunications (BUPT), Beijing, China, in 2009, and the Ph.D. degree in communication and information systems from NUPT in 2023. His research interests are in the areas of next-generation broadband networks and wireless communication systems, with an emphasis on analysis of non-orthogonal multiple access (NOMA) and stochastic geometry applied to wireless systems.

**Martin Haenggi** (Fellow, IEEE) received the Dipl.-Ing. (M.Sc.) and Dr.sc.techn. (Ph.D.) degrees in electrical engineering from the Swiss Federal Institute of Technology Zurich (ETHZ) in 1995 and 1999, respectively. Currently, he is a Freimann Professor in electrical engineering and a Concurrent Professor in applied and computational mathematics and statistics with the University of Notre Dame, IN, USA. In 2007 and 2008, he was a Visiting Professor with the University of California at San Diego, in 2014 and 2015, he was an invited Professor with EPFL, Switzerland, and in 2021 and 2022, he was a Guest Professor with ETHZ. He is the co-author of the monographs *Interference in Large Wireless Networks* (NOW Publishers, 2009) and *Stochastic Geometry Analysis of Cellular Networks* (Cambridge University Press, 2018) and the author of the textbook *Stochastic Geometry for Wireless Networks* (Cambridge, 2012) and the blog stogblog.net. His scientific research interests lie in networking and wireless communications, with an emphasis on cellular, amorphous, ad-hoc (including D2D and M2M), cognitive, vehicular, and wirelessly powered networks. For both the M.Sc. and Ph.D. theses, he was awarded the ETH medal. He also received the CAREER Award from the U.S. National Science Foundation in 2005 and three paper awards from the IEEE Communications Society, the 2010 Best Tutorial Paper Award, the 2017 Stephen O. Rice Prize Paper Award, and the 2017 Best Survey Paper Award. He is also a Clarivate Analytics Highly Cited Researcher. He served as an Associate Editor for the *Ad Hoc Networks* (Elsevier), IEEE TRANSACTIONS ON MOBILE COMPUTING (TMC), and *ACM Transactions on Sensor Networks*; as a Guest Editor for the IEEE JOURNAL ON SELECTED AREAS IN COMMUNICATIONS, IEEE TRANSACTIONS ON VEHICULAR TECHNOLOGY, and the *EURASIP Journal on Wireless Communications and Networking*; as a Steering Committee Member for IEEE TRANSACTIONS ON MOBILE COMPUTING; and as the Chair of the Executive Editorial Committee for IEEE TRANSACTIONS ON WIRELESS COMMUNICATIONS (TWC). From 2017 to 2018, he was the Editor-in-Chief of IEEE TRANSACTIONS ON WIRELESS COMMUNICATIONS.

**Qi Zhu** received the bachelor's and master's degrees in radio engineering from Nanjing University of Posts and Telecommunications (NUPT), Nanjing, China, in 1986 and 1989, respectively. She is currently a Professor with the School of Telecommunication and Information Engineering, NUPT. Her research interests include technology of next-generation communication, broadband wireless access, orthogonal frequency division multiplexing, channel and source coding, and allocation of radio resources.

**Caili Guo** (Senior Member, IEEE) received the Ph.D. degree in communication and information systems from Beijing University of Posts and Telecommunications (BUPT), Beijing, China, in 2008. She is currently a Professor with the School of Information and Communication Engineering, BUPT. Her general research interests include machine learning and statistical signal processing for wireless communications, with current emphasis on multimedia computing and mobile edge intelligence for the Internet of Vehicles.

**Yifei Yuan** (Fellow, IEEE) received the bachelor's and master's degrees from Tsinghua University, China, and the Ph.D. degree from Carnegie Mellon University, USA. He was with Alcatel-Lucent from 2000 to 2008. From 2008 to 2020, he was with ZTE Corporation as a Technical Director and a Chief Engineer, responsible for standards & research of 4G LTE-advanced and 5G technologies. He joined China Mobile Research Institute in 2020 as a Chief Expert, responsible for 6G wireless research. He has extensive publications, including ten books on LTE-advanced, 5G, and 6G. He has over 60 granted U.S. patents.

**Zhuhua Hu** (Senior Member, IEEE) received the B.E. and M.E. degrees from Jilin University, Changchun, China, in 2002 and 2005, respectively, and the Ph.D. degree from Hainan University, Haikou, China, in 2019. Since 2020, he has been a Professor with the School of Information and Communication Engineering, Hainan University. He is currently a high-level talent in Hainan Province. His research interests include artificial intelligence and signal and information processing.

**Xiaohui Li** (Member, IEEE) received the Ph.D. degree in communication and information system from the School of Telecommunication and Information Engineering, Nanjing University of Posts and Telecommunications (NUPT), Nanjing, China. She was also a Visiting Student with the Department of Electrical and Computer Engineering, Western University, London, Canada, in 2018. She is currently a Faculty Member with the School of Telecommunication and Information Engineering, NUPT. Her current research interests include integrated sensing and communication, reconfigurable intelligent surface, crowd sensing, and dynamic spectrum access and sharing.